ERDC/CRREL TR-23-4

US Army Corps
of Engineers®
Engineer Research and
Development Center

ERDC
ENGINEER RESEARCH & DEVELOPMENT CENTER

Analysis of Paxton Siphon Frazil Ice Blockage Event during January 2022

Chandler Engel, Jeremy Giovando, and Grant Halvorson

May 2023

Cold Regions Research
and Engineering Laboratory

The US Army Engineer Research and Development Center (ERDC) solves the nation's toughest engineering and environmental challenges. ERDC develops innovative solutions in civil and military engineering, geospatial sciences, water resources, and environmental sciences for the Army, the Department of Defense, civilian agencies, and our nation's public good. Find out more at www.erdc.usace.army.mil.

To search for other technical reports published by ERDC, visit the ERDC online library at https://erdclibrary.on.worldcat.org/discovery.

ERDC/CRREL TR-23-4
May 2023

Analysis of Paxton Siphon Frazil Ice Blockage Event during January 2022

Chandler Engel and Jeremy Giovando

US Army Engineer Research and Development Center
Cold Regions Research and Engineering Laboratory
72 Lyme Road
Hanover, NH 03755

Grant Halvorson

US Army Corps of Engineers
St. Paul District
332 Minnesota St, Suite E1500
St. Paul, MN 55101

Final report

Prepared for Nebraska Public Power District
1414 15th St
Columbus, NE 68602

Under MIPR 5J238-19L5JL

Abstract

In early January 2022, the Paxton Siphon, owned and operated by the Nebraska Public Power District, filled with frazil ice creating a blockage that resulted in a rapid upstream stage rise for the Sutherland Canal. An event of this type has never happened in the over 80 years of operating the Paxton Siphon. An analysis of the available weather and canal data suggests a rapid air temperature change resulted in the water becoming supercooled, which combined with the moderately low flows in the canal resulted in an anomalous frazil ice formation event. To address this issue for future cold-weather events, a water-temperature model was developed using the Hydrologic Engineering Center's River Analysis System and can be used to determine the spatial extents of the supercooling event using forecasted weather information. In addition, we developed a heat-exchange forecast tool that can be used operationally to screen for potential frazil ice formation periods with a 1-week outlook period.

Contents

Figures and Tables

Figures

Tables

Preface

This study was conducted for the Nebraska Public Power District under MIPR 5J238-19L5JL. The technical monitor was Mr. Edward Dekleva.

The work was performed by the Terrain and Ice Engineering Group (Dr. Meghan Quinn, lead) of the Remote Sensing/GIS Center of Expertise (Mr. David Finnegan, center director), US Army Engineer Research and Development Center, Cold Regions Research and Engineering Laboratory (ERDC-CRREL). At the time of publication of this report, the acting deputy director of ERDC-CRREL was Dr. Ivan P. Beckman, and the director was Dr. Joseph L. Corriveau.

The authors appreciate all the reviewers; their comments were constructive and helped to improve this document.

The commander of ERDC was COL Christian Patterson, and the director was Dr. David W. Pittman.

This page intentionally left blank.

1 Introduction

1.1 Background

The initial ice-cover formation process on natural waterbodies is principally controlled by supercooling of water (USACE 2002). Supercooling of freshwater occurs when the temperature drops below 0°C (32°F).[1] While air temperature is a key variable in this process, other variables can also be important for determining the amount of supercooling that occurs. Depending on the water body type (e.g., lake or river), windspeed and water velocity will also be important factors. In quiescent waterbodies, growth of ice cover through thermally driven processes will dominate when there are subfreezing temperatures. Examples include lakes or ponds during low-wind conditions or in streams with flow velocity of 0.3 m/s (1 ft/s) or less (USACE 2002). The initiation of ice will be from seed crystals falling from the atmosphere into a very thin surface layer of supercooled water. Ice will continue to grow in a columnar shape at the interface boundary between the ice and water as heat is transferred upward toward the colder atmosphere.

In contrast, lakes and rivers with water-surface turbulence will experience mixing of the thin layer of supercooled water within the water column. In rivers and streams, this can result in complete mixing and supercooling of the entire water column. In this situation, the seed crystals will create nucleation of frazil ice crystals (disk shaped). Seed crystals are often formed from atmospheric water vapor, or spray from waves. Once nucleation of ice occurs in supercooled water, secondary nucleation will quickly generate substantially more ice crystals, which are usually held in suspension in the moving water. Secondary nucleation will continue until enough latent heat is released through the water-ice phase change to warm the surrounding water to 0°C (32°F). As the frazil ice concentration increases, ice crystals adhere to one another, forming flocs and ultimately floes that will be visible on the water surface. Frazil ice generation will continue while open-water conditions persist. Once ice cover is formed,

[1] For a full list of the spelled-out forms of the units of measure and unit conversions used in this document, please refer to *US Government Publishing Office Style Manual*, 31st ed. (Washington, DC: US Government Publishing Office 2016), 248–52 and 345–7, respectively. https://www.govinfo.gov/content/pkg/GPO-STYLEMANUAL-2016/pdf/GPO-STYLEMANUAL-2016.pdf.

then transport of frazil ice underneath the ice cover can occur. The process of developing ice cover from frazil ice is shown in Figure 1 (Daly 1984).

Figure 1. Evolution of frazil ice in natural water bodies (Daly 1984).

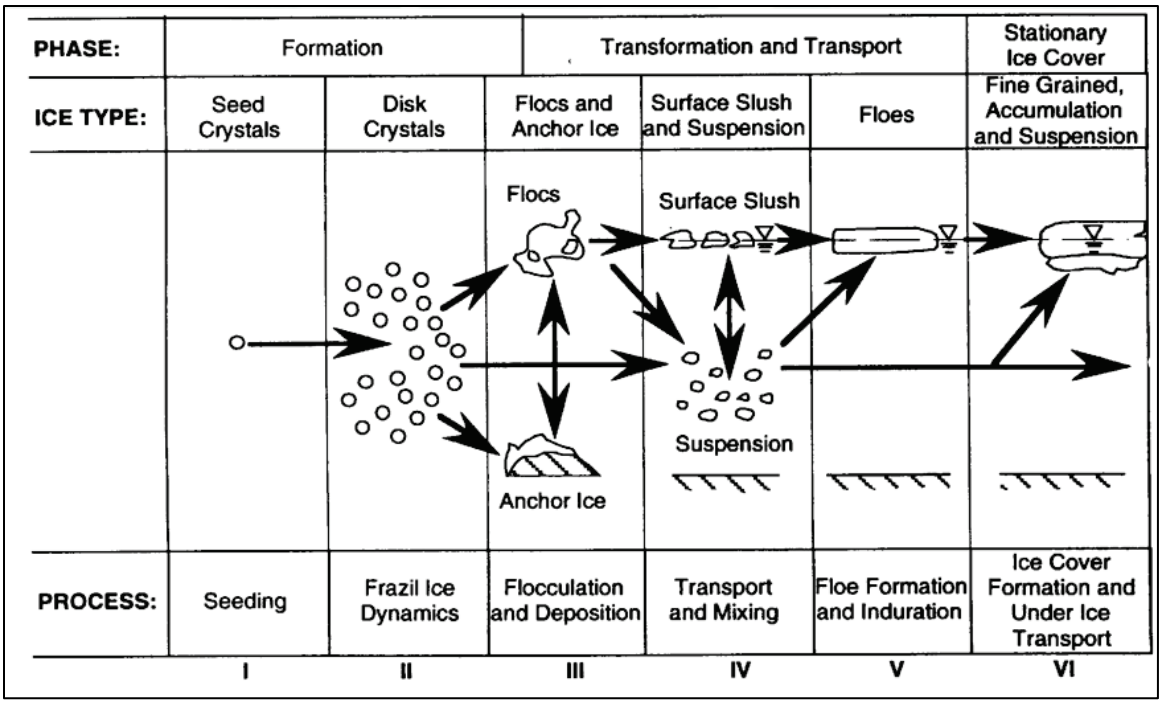

Ice can result in several problems including ice jams, additional loading on structures, blockage of water intakes, hydroelectric plant intakes, and irrigation canals (Daly 1984). Ice jams and blockage of intakes and canals are operational issues that challenge water managers. Ice jams occur when the ice transport capacity of the river or stream is exceeded (USACE 2002). Areas prone to ice jams are locations where there is a channel obstruction or change in geometry that affects the hydraulic characteristics of the flow. Ice jams form during both freeze-up and breakup of ice cover. Freeze-up ice jams are associated with frazil ice accumulation while breakup jams are usually a result of ice fragments accumulating during changes in streamflow due to rainfall or snowmelt (Beltaos 1995; USACE 2002). In rivers, streams, and canals, high concentrations of frazil ice can result in a freeze-up ice jam that will increase the upstream stage and potentially lead to flooding of areas adjacent to the channel (Daly 1984). Frazil ice accumulation on trash racks is one challenge associated with operating water and hydroelectric intakes in cold regions (Daly and Ettema 2006; Dean 1983; Gebre et al. 2013). Another challenge is the accumulation and generation of frazil ice within intake pipes, power penstocks, and other pressurized conduit structures (Ettema et al. 2009).

When water is pressurized, the freezing temperature threshold is depressed and can result in melting of ice entering the conduit while simultaneously supercooling the water flowing through the conduit. Once the pressure is reduced, rapid frazil ice formation occurs that can result in partial or complete blockage at the downstream end of the conduit (Ettema et al. 2009). Modeling the ice and flow interaction within the pressurized conduit requires a detailed computational fluid dynamics model.

Due to the challenges that frazil ice creates for water-management activities, the formation, modeling, and prediction of frazil ice have been addressed by several publications (Andersson and Daly 1992; Ashton 1983; Carstens 1970; Daly 1994; Daly 1984; Ettema et al. 1984; Richard et al. 2015). The numerous laboratory studies of frazil ice summarized by Barrette (2020) suggests we have a reasonable understanding of how frazil ice is formed; however, there still are open questions related to modeling and predicting frazil ice accumulation in rivers, streams and canals. Ettema et al. (1984) provide the mathematical formulations to combine both heat transfer theory with elements of turbulence theory. Ice formation using this mathematical formulation has been implemented in hydrodynamic models like River1D (Blackburn and She 2019) and RIVICE (Lindenschmidt 2017). The challenge, as discussed by Blackburn and She (2019), is that parameterization and calibration of the model requires ice observations. Even when measurements of frazil ice are available, there are still challenges relating those measurements to model parameters (Richard et al. 2015).

Other approaches to modeling river ice have used water-temperature models to estimate timing and location of ice formation. Morales-Marín et al. (2019) used a one-dimensional (1D) water-temperature model to simulate the timing of river freeze-up for the Athabasca River in Canada. Giovando et al. (2019) again used a 1D temperature model to estimate ice timing and location on the Pend Oreille River in Idaho using the River Analysis System (RAS) (Brunner 2016) software developed by the Hydrologic Engineer Center (HEC).[2] Using water temperature without the ice formation processes has limitations especially when evaluating the accumulation of ice and the associated feedback on the hydrodynamics. However, as discussed in Giovando et al. (2019), water managers often need forecast tools that can be used with only a few input variables so

[2] The software is commonly referred to as *HEC-RAS*.

operational decisions can be made in a timely manner. This suggests that 1D water-temperature models can be helpful when evaluating frazil ice formation in a system that is accurately represented by a tool like the HEC-RAS.

1.2 Study Area

The study area is contained within Keith County, Nebraska. Water levels in Lake McConaughy and Lake Ogallala are controlled by Kingsley Dam hydropower releases and Keystone Diversion Dam, respectively. The Nebraska Public Power District's (NPPD) Sutherland Canal routes water alongside the North Platte River from Lake Ogallala to Sutherland Reservoir and the Gerald Gentleman Station, approximately 53.1 km (33 miles) downstream. In Paxton, Nebraska, the Sutherland Canal feeds water into a 2.3 km (1.4 mile) siphon that conveys water beneath the South Platte River and other infrastructure within the city (Figure 2).

Hydraulic modelling efforts focus on a 27.5 km (17.1 mile) reach of the Sutherland canal ranging from a gage 2.6 km (1.6 miles) downstream of Keystone Diversion Dam to the entrance of the Paxton Siphon (Figure 2).

The Sutherland Canal from Lake Ogallala to the siphon contains a total of 6.4 km (4.0 miles) of lined channel and 23.7 km (14.7 miles) of unlined channel. The lined channel is generally characterized by a concrete lining while the unlined channel generally contains riprap. Monitoring locations where NPPD collects stage, water temperature, and flow information are labeled by the mile post (MP) designation (Figure 2).

Figure 2. Map of study area with River Analysis System (RAS) model extents. Stage and temperature monitoring locations are included along with lined sections of the canal. Hydrologic Engineering Center–River Analysis System (HEC-RAS) model stations in parentheses.

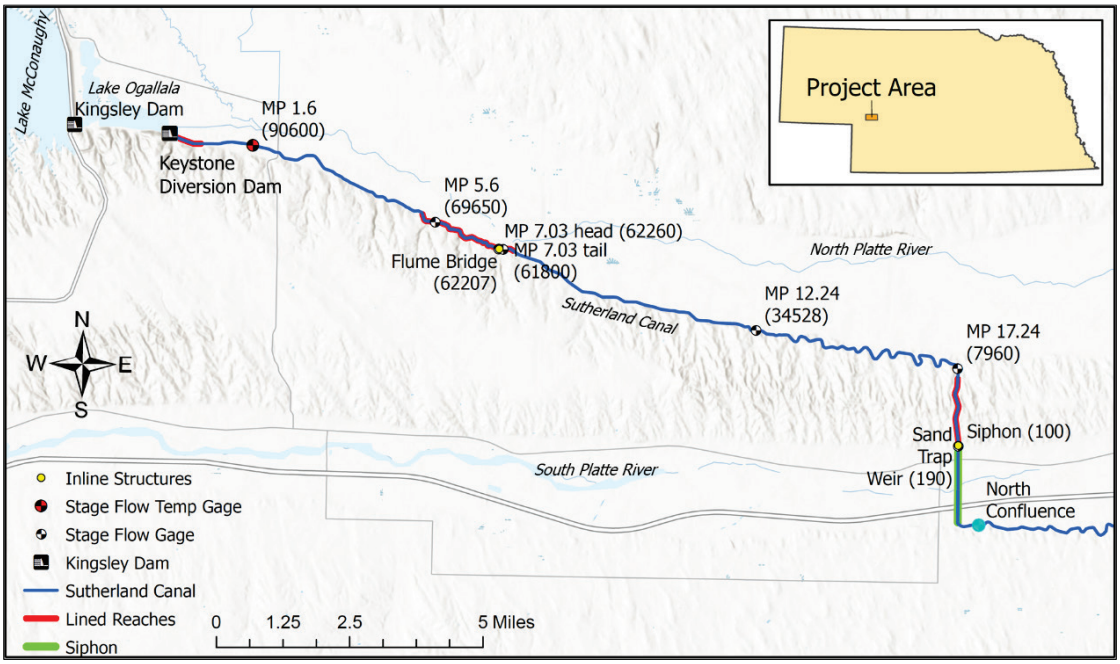

1.3 Regional Climate

Climate data are available at two airports near the study area. Ogallala Municipal Airport (OGA) is 35.4 km (22 miles) west of the siphon. North Platte Airport is 54.7 km (34 miles) east of the siphon. A summary of daily air temperature for the period of Water Year (WY) 1997–2022 is shown in Figure 3. The mean, 90% exceedance, and 10% exceedance for the mean daily values are also included to show the range of air temperatures for each season. For the winter months of December through March, daily air temperature below freezing is common. In contrast, the summer air temperatures average near 25°C (77°F).

Figure 4 summarizes the relative humidity (RH) from the OGA. There is not a large range in average RH, but seasonal differences are still apparent. The highest RH is for the winter months while, conversely, the lowest RH is during the summer months (Figure 4). Monthly wind rose plots for December through February at OGA are shown in Figure 5. Due to the seasonality of ice formation in the Sutherland Canal, we limit the wind rose plots to months with the highest probability of ice formation. The December wind events are most commonly from the west while the highest windspeeds are mostly from the northwest directions (Figure 5*A*). January has a similar wind-direction pattern with a few more occurrences

of higher windspeed events (Figure 5*B*). In February, the predominant wind direction is consistent with December and January; however, there are a few moderate-speed wind events that do come from the east and southeast directions (Figure 5*C*).

Based on climate data for our study site, there are commonly subfreezing temperatures occurring during the December-through-February period with high winds coming from the north or northwesterly directions. During the winter season, storms coming from the north can have the potential for extreme cold temperatures for several days. These weather conditions are a key component in the formation of frazil ice for the Sutherland Canal.

Figure 3. Summary of mean daily air temperature for Ogallala Municipal Airpost (OGA) (Water Year [WY] 1997–2022).

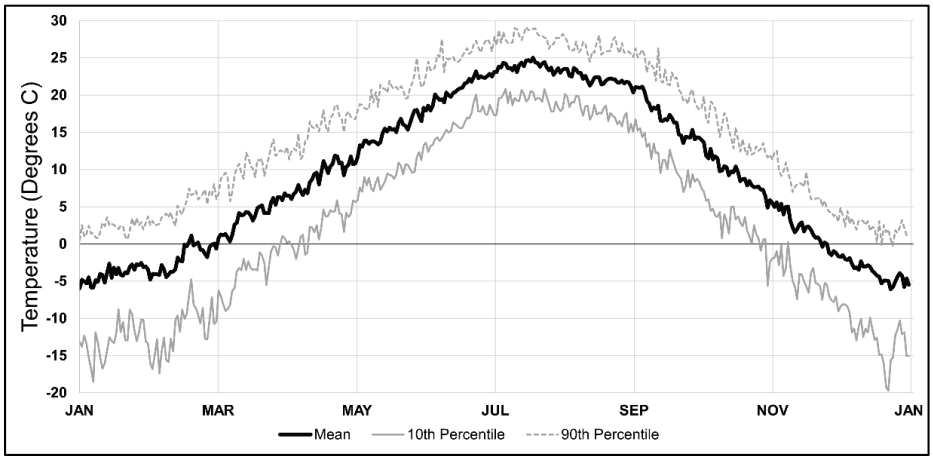

Figure 4. Summary of relative humidity measurements at OGA (WY 1997–2022).

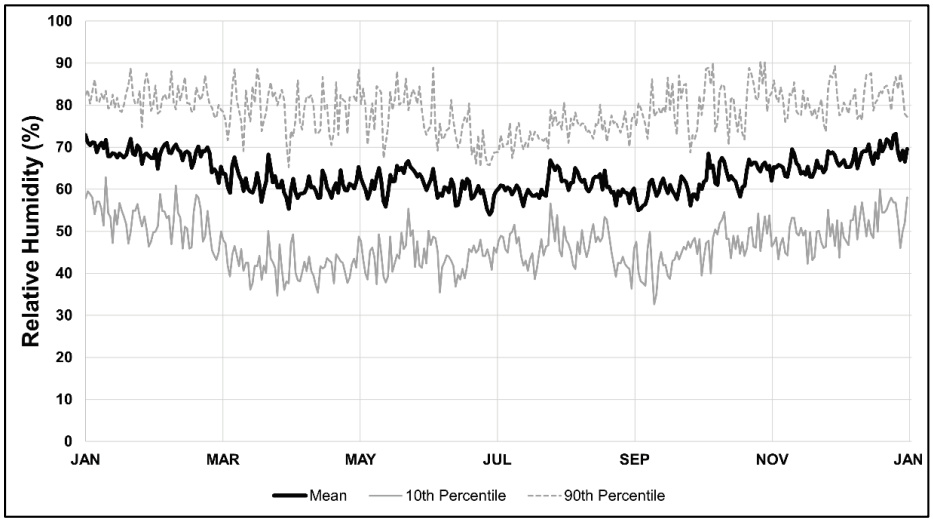

Figure 5. Summary of winter windspeed and direction for OGA (WY 1997–2022). Plots produced from Iowa Environmental Mesonet (ISU 2022).

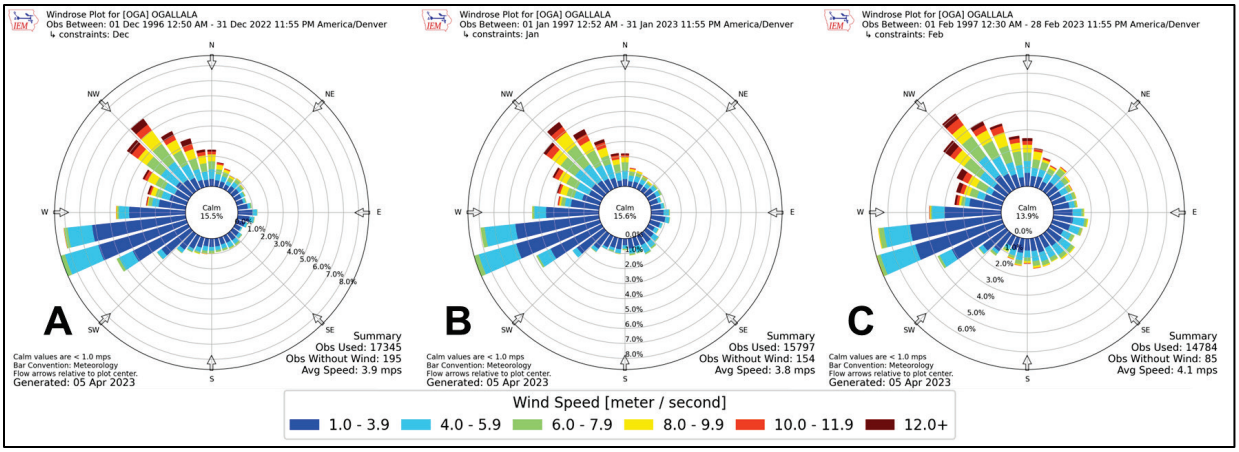

1.4 Objectives

The overall objectives of our study were to identify the conditions that resulted in the blockage of the Paxton Siphon at around 0645 on 6 January 2022 and create a tool to evaluate potential frazil ice formation from future extreme cold events. Specific objectives included the following:

- Document ice and weather conditions during the January 2022 event and put that event in historical context.
- Develop a prediction tool using weather forecasts and a water-temperature model to help NPPD operations staff evaluate potential frazil ice formation.

1.5 Approach

In this study, our approach was to use regional weather data and water-temperature measurements collected in the Sutherland Canal to put the January 2022 frazil ice event in the context of previous cold periods. Then using the historical information, we developed a water-temperature forecast model that can be used operationally by NPPD staff to make internal preparations for monitoring and potential operational changes to the canal.

Many of the methods, particularly the heat transfer modeling, used in our analysis were originally derived using SI units (metric), and equivalent equations for Imperial units have not been developed. However much of the input information, along with the hydraulic model, provided by NPPD

were in Imperial units. Therefore, we have generally performed this analysis using SI units, but we report the Imperial equivalent for some values, such as water flow rates and distances, to provide clarity or association with information provided to us for this effort.

1.6 Scope

The scope of our study was limited to the Sutherland Canal above the Paxton Siphon. Analysis of Lake Ogallala ice cover was also performed to provide qualitative information about water temperature entering the Sutherland Canal. Due to complexity of modeling frazil ice concentrations and lack of observational data related to supercooling of the water in the canal, we focused our efforts on developing tools that can be used by NPPD to help with future water management decisions. Direct modeling of frazil ice is feasible with hydrodynamic tools still under development at research institutions. However, the data requirements and inability to validate parameters (due to the lack of frazil ice observations) make using those models beyond the scope of the current study.

2 Summary of January 2022 Paxton Siphon Blockage Event

2.1 Weather Conditions

We compared daily average air temperature values for the January 2022 event with the summary air temperature values from Figure 3. The air temperature values leading into the event were above normal for the season and then dropped quickly as the cold front moved into the area (Figure 6). The 1 January 2022 daily average temperature was below the 10th percentile value by approximately 3°C (5.4°F). There was a brief rebound in air temperature to above-normal temperature prior to the next cold front coming into the region. The air temperatures from 5 to 7 January were again much below average. Following the siphon blockage, the air temperatures on 8–13 January warmed to above-average temperatures and exceeded the 90th percentile daily temperature values on 13 January (Figure 6).

Figure 6. Daily average air temperature for OGA from December 2021 through January 2022. Percentiles computed from December through March daily average air temperatures for WY 1997 to 2022.

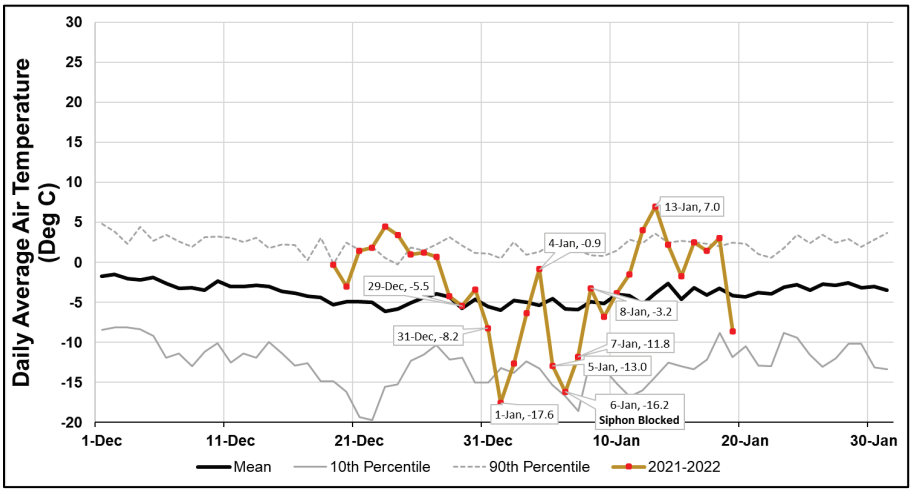

We can further put the severity of the January 2022 event into historical context by plotting the nonexceedance probability using daily average air temperature values from WY 1997–2022. The coldest days (1 January and 5 January) from the back-to-back, below-average temperature periods have a nonexceedance value of less than 5% (Figure 7). This indicates that only 5% of the historical daily average air temperature values in the past 26 yr are less than those 2 days. Several of the days during early January

2022 have nonexceedance values less than 25% (Figure 7), indicating this period was certainly cold, but it was not record breaking even within the last 26 yr.

Figure 7. Daily average air temperatures from January 2022 event with percent nonexceedance values for December through March OGA daily average air temperature between WY 1997 and 2022.

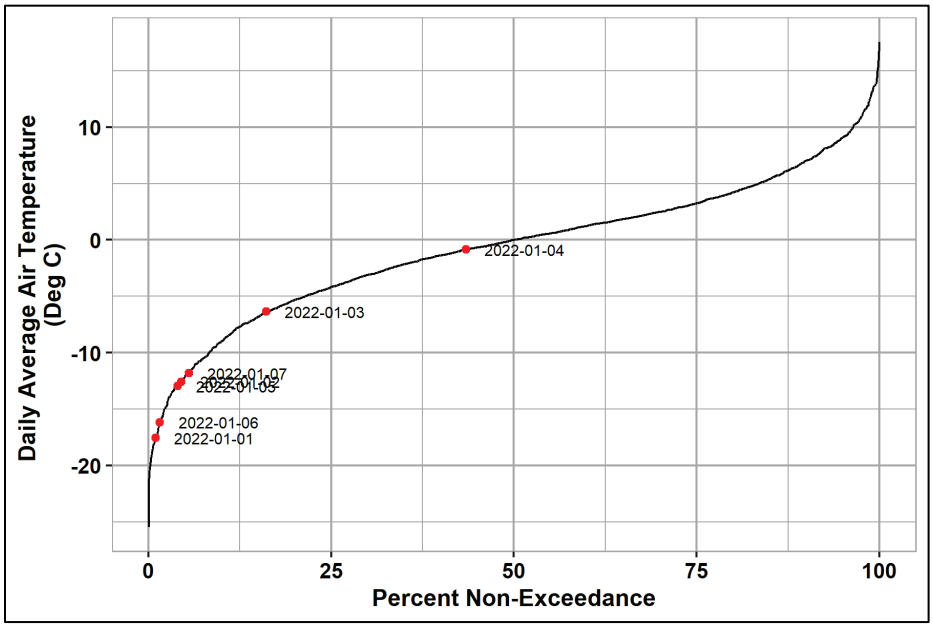

2.2 Observed Stages and Action Taken by Nebraska Public Power District (NPPD)

Stage data collected by NPPD during the January 2022 event also provides information about how the ice formation on the canal progressed. The initial cold period of 31 December through 2 January indicates some ice formation on the canal resulted in stage increases for locations downstream of MP 7.03 (Figure 8). The stage changes during this period were not substantial, indicating the overall ice effects were minimal. During the brief warm-up in temperatures on 4 January, all ice affects appear to be gone from stage records except for the North Confluence site (Figure 8). This suggests that leading into the cold period that caused the siphon blockage, ice cover upstream of the siphon was decreasing while the ice cover downstream of the siphon remained in place.

The second period of cold weather occurred on 5–7 January 2022, which significantly impacted canal stage downstream of MP 7.03. The largest stage increase occurred at the siphon entrance followed by MP 17.24 with

over 3 m (9.8 ft) of change (Figure 8). During this period, approximately 12.7 cms (450 cfs) was flowing through the Paxton Siphon. As discussed in the NPPD letter to the Federal Energy Regulatory Commission (FERC),[3] ice accumulation in the Paxton Siphon increased to levels that reduced hydraulic capacity starting near 0645 on 6 January. The increased stage levels upstream were discovered by canal patrol staff approximately 7.5 hr later. In response to the increased stage upstream of the siphon, operators ceased diversions from Lake Ogallala and opened wasteway gates on the canal. Local emergency management officials along with FERC were notified shortly after discovering the issue.

The NPPD inspection of the siphon following the shutdown of flows revealed substantial portions of the siphon were filled with ice. They report that during the 23 January inspection, more than 2 weeks after the event, ". . . a majority or more of the river section contained ice; however, the invert of the siphon was generally clear of ice . . ."[4] In late January, diversions from Lake Ogallala were reinitiated without incident, and normal operating service was reached by 1 February.[5]

Figure 8. Observed stages at Nebraska Public Power District (NPPD) gages during January 2022 event. Locations include gages immediately below the siphon upstream to mile post (MP) 1.6 on the Sutherland Canal.

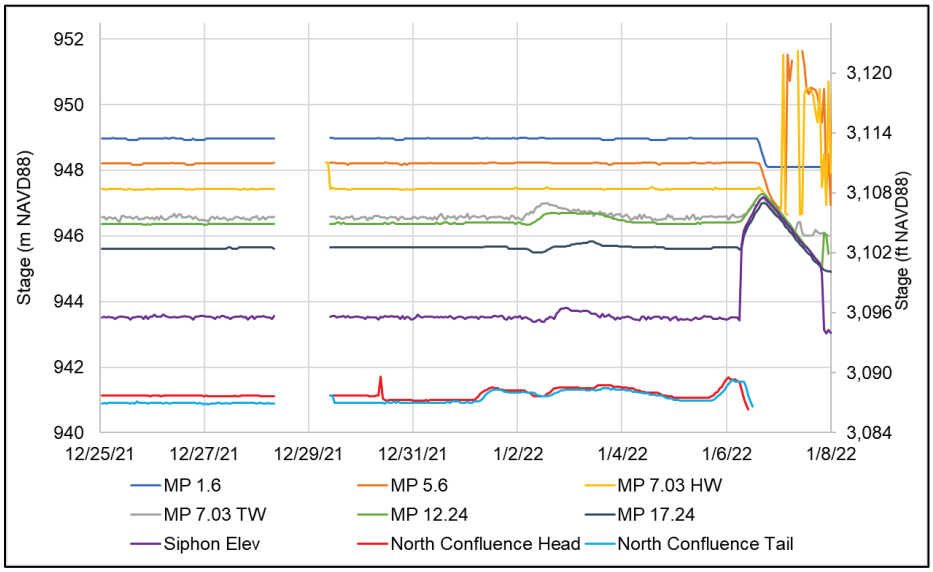

[3] NPPD (Nebraska Public Power District). 2022. Letter to Federal Energy Regulatory Commission, March 1.

[4] NPPD 2022.

[5] NPPD 2022.

3 Methods and Data

3.1 Stage and Flow Data

There are seven gages with stage and flow readings within this reach, including a gage at the upstream portion of the modeling reach that records stage, flow, and temperature. The data records available from the NPPD database are summarized in Figure 9. The water-temperature data were the limiting dataset in our analysis.

Figure 9. Period of record for stage (*black*), flow (*blue*), and temperature (*red*) available for the Sutherland Canal from the NPPD database. Incomplete or poor-quality temperature data were flagged (*light red*).

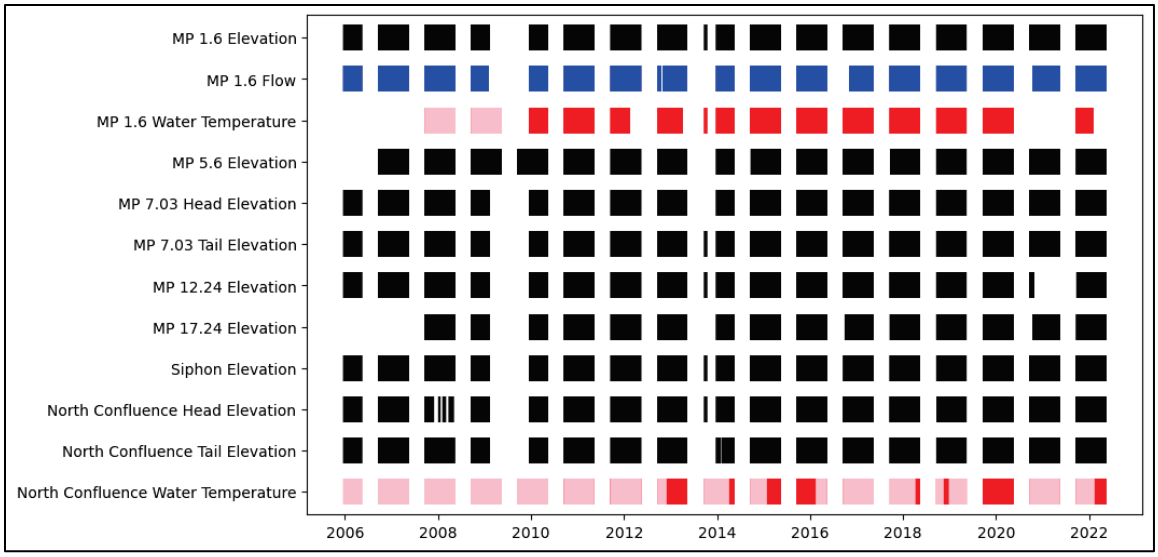

3.2 Climate Data

Several sources of climate data were used in our analysis. The hourly air temperature, cloudiness, air pressure, humidity, and windspeed data from the OGA (location identifiers Weather Bureau Army Navy 94063 and US Air Force 725621) were used directly within the water temperature modeling. Other data were used for validation of model assumptions. Specifically, net incoming radiation from an NPPD employee's home weather station was compared against the values computed by the water temperature model for validation.

3.3 Remote Sensing Data

Images from the PlanetScope constellation of Dove satellites were used to evaluate ice cover on the canal and Lake Ogallala prior to the 2022 event (Planet Developers 2023). Quantitative applications of remote sensing data for frazil ice concentrations were not feasible. Therefore, we were not able to utilize this information directly in the water temperature forecast tool development.

3.4 Summary of Annual Ice Events

Using the stage records from WY 2006–2022, we determine the ice-affected stage events for both the Paxton Siphon and other locations on the Sutherland Canal. These events were identified through visual inspection of the stage records. To be considered an ice-affected stage event, the characteristic sharp drop followed by a rapid rise in stage was used for identification. An example of this characteristic pattern is highlighted in Figure 10.

Figure 10. Example of the characteristic ice-affected stage used to identify events using the NPPD stage records for Sutherland Canal.

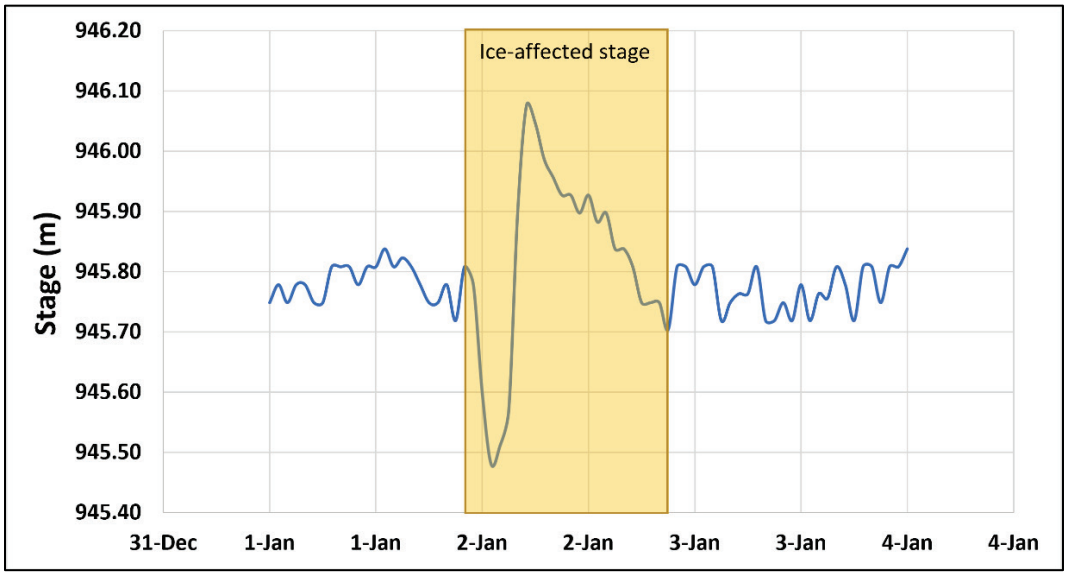

3.5 Hydraulic Modeling

The Sutherland Canal hydraulic model used for this study was originally developed by NPPD for operational and dam safety studies. It is a 1D HEC-RAS model that was originally calibrated using unsteady flows entering into the canal from Lake Ogallala. The model was originally developed,

and all calibration was done in HEC-RAS version 6.1.0. The average distance between cross sections was 6.1 m (20 ft), and there was a total of 4,944 cross sections between Lake Ogallala and the Paxton Siphon. Gages, structures, and locations in the hydraulic model we used in this study are summarized in Table 1.

Table 1. Gages, structures, and their locations in the hydraulic model.

Name	Type	RAS Station
MP 1_6	Stage and Flow and Temperature Gage	90600
—	Bridge	69652
MP 5_6	Stage Gage	69600
MP 7_03 Headwater (HW)	Stage Gage	62260
Flume Bridge	Inline Structure	62207
MP 7_03 Tailwater (TW)	Stage Gage	61800
MP 12_24	Stage Gage	34528
—	Bridge	34526
MP 17_24	Stage Gage	7980
—	Bridge	7958
Sand Trap Weir	Inline Structure	190
Siphon Elevation	Stage Gage	100
Siphon Inlet	Boundary Condition	0
North Confluence	Stage (HW/TW) and Temperature	~ −10000 (not in model)

For our study, we used the original HEC-RAS model as a foundation but performed several key changes to optimize the model performance for winter flow conditions. The number of cross sections were reduced to a total of 918 between Lake Ogallala and the Paxton Siphon. This reduced runtime while still maintaining the spatial resolution to accurately represent the canal stage at all locations in our study reach.

In addition, the parameters were adjusted from the original model. These parameters reflect observed stages during winter conditions when vegetation effects in the canal are minimal. Using only winter periods, we determined parameter adjustments for each reach in the canal. Channel roughness values were changed uniformly within each lined and unlined reach for our model calibration process. This approach provides a physical

basis for modifying the channel roughness values. The adjusted roughness parameters were determined through calibrating for the winter flow periods of WY 2018–2022. Our calibration approach assumes the previously calibrated roughness values are a good *all-season* fit for the Sutherland Canal, and we only need to modify reaches that have larger error during winter flow conditions. Without a detailed record of when the canal was either ice covered or in an open-water condition, the calibration represents average, or typical winter conditions, and does not explicitly account for the presence of an ice cover.

Other modifications to the original hydraulic model provided by NPPD included lengthening the model time-step from 10 sec to 1 min. Again, this was done to reduce compute time for simulations. We also adjusted the location of the upstream boundary cross section. The original model used the outlet of Lake Ogallala into the Sutherland Canal as the upstream boundary location. For our analysis, the first location with stage and temperature data was at MP 1.6 (approximately 2,600 m [8500 ft] downstream); therefore, we used this cross section as the upstream boundary for all our model simulations.

3.6 Water Temperature Modeling

3.6.1 Hydrologic Engineering Center–River Analysis System (HEC-RAS) Water Quality Module

The Water Quality Module (WQM) in HEC-RAS has the capability to simulate temperature between cross sections along the length of a hydrodynamic model by calculating and summing the components of the energy balance. HEC-RAS version 5.0.7 was used to rerun the hydraulics and the water quality model due to issues with WQM in version 6.1.0. The simulation estimates the following energy sources and sinks:

- energy gained from shortwave solar radiation, including effects of cloud cover
- longwave radiation absorbed from the atmosphere
- longwave radiation emitted by the water body
- sensible heat exchange between the water and air, including the effects of wind
- latent heat from evaporation and condensation at the water surface

The HEC-RAS User's Manual provides detailed information about the methods used to calculate the components of the energy balance along with details about parameterizing the model (Brunner 2016).

The model requires detailed meteorological input data to calculate the individual heat flux terms including the following:

- air temperature
- windspeed
- portion of the sky covered in clouds
- relative humidity
- atmospheric pressure

Most of these data are obtained from the automated surface observation system (ASOS) network, which is typically located at airports (NWS, "ASOS," n.d.). Data about the portion of the sky covered by clouds are not directly available through ASOS, so we derived the cloud-cover parameter by decoding Meteorological Aerodrome Reports (METAR) messages in the ASOS data that describe cloud cover in terms of *oktas*, or $^1/_8$ segments of the sky. The obstructed fraction used in this analysis (Table 2) was interpreted from the official description of the METAR codes (FAA 2016).

Table 2. Cloud fraction used in water temperature model (FAA 2016).

METAR Code	Meaning	Cloud-Obstructed Oktas	Obstructed Fraction
SKC or CLR	Clear	0	0.0000
FEW	Few	1/8–2/8	0.1875
SCT	Scattered	3/8–4/8	0.4375
BKN	Broken	5/8–7/8	0.7500
OVC	Overcast	8/8	1.000

ASOS data for the OGA were automatically downloaded from the Iowa State Mesonet application programming interface (API) using a Python script and converted to the HEC-data storage system (DSS) format for use in HEC-RAS (Brunner 2016). Data from the Nebraska ASOS sites are available for manual download as well: https://mesonet.agron.iastate.edu/request/download.phtml?network=NE_ASOS.

An example of input data used in the HEC-RAS WQM, herein referred to as the *water temperature model*, is shown in Figure 11.

Figure 11. Example input meteorological time-series data for the HEC-RAS, water temperature model.

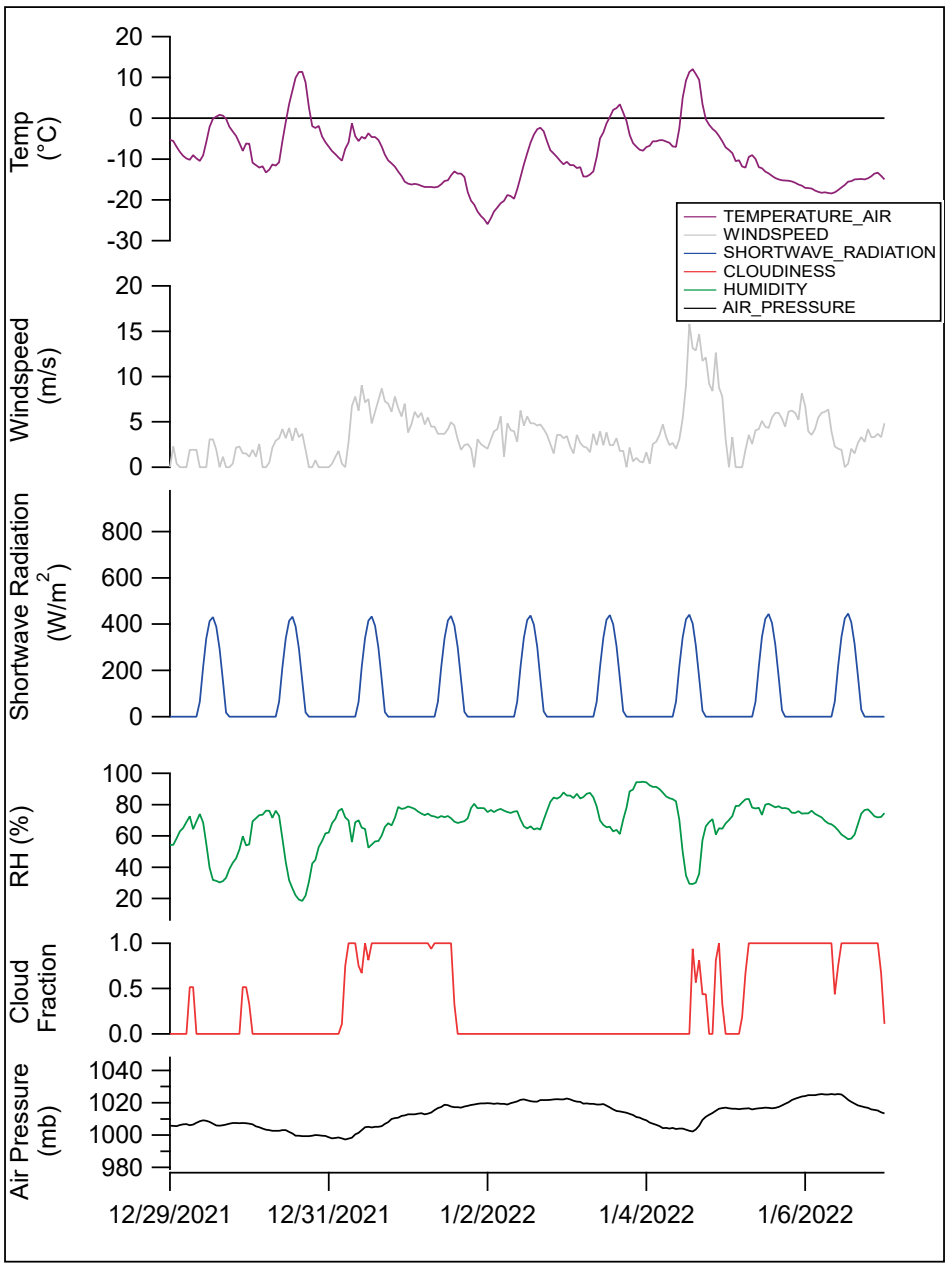

The temperature model simulates the effect of the calculated heat fluxes on discrete volumes of water in cells defined by pairs of cross sections. The hydrodynamic portion of the model is run first, and the temperature model runs on the postprocessed data, which accounts for advection of heat as water flows through the model while simultaneously being exposed to energy sources and sinks in the atmosphere. The model does not account for energy losses to the canal walls.

Output from the model includes modeled temperature at each water quality cell. Each cell is defined as the zone between a pair of cross sections, and in this study were set to a minimum of 91.4 m (300 ft) long, therefore spanning four hydraulic cross sections typically spaced 30.5 m (100 ft) apart (Table 3). The temperature model uses a dynamic time-step and output from the simulation was recorded at 15 min intervals. From these data, the location of canal sections that approach and reach the freezing temperature can be identified. The model does not directly account for the significant heat exchanges that occur during ice formation, particularly the release of latent heat when water transitions from liquid to solid ice. The model also does not account for the influence of an ice cover, either from thermally grown ice or accumulated frazil ice. An ice cover will significantly change the heat exchange between the water and the air (e.g., by blocking solar radiation, limiting the release of longwave radiation, and reducing the impact of sensible heat transfer from differences in water and air temperature). However, the assumptions made in the model are appropriate for conditions that typically lead up to frazil ice-generating events when water bodies are generally ice free.

Table 3. Partial listing of hydraulic and water temperature model parameters.

Parameter	Value	Units
Hydraulic model time-step	1	minute
Water temperature model time-step	Dynamic 11.9–15.2	second
Hydraulic model cross-section spacing	30.5 (100)	m (foot)
Water temperature model cross-section spacing	91.4 (300) (minimum)	m (ft)

3.6.2 Sutherland Canal Water-Temperature Model

The primary focus of temperature modeling in this study was a simulation of the Sutherland Canal starting at MP 1.6 to the siphon entrance. Water temperature downstream of the siphon was not evaluated since frazil ice generation upstream is considered to have the most direct impact on potential flow blockage events.

The temperature model requires a specified water temperature boundary condition at the upstream end. There are two locations where water temperature is measured, at MP 1.6 and at the North Confluence (Figure 2). The observed hourly water temperatures at MP 1.6 were used for the

upstream boundary condition for the water temperature model. The model ends at the siphon entrance; however, the calculated temperatures at the last section of the model were compared to values at the North Confluence to evaluate model performance. The utility of the North Confluence temperature data was limited, however, because it was (1) daily averaged temperatures and (2) had intermittent quality. We were able to isolate WY 2019 and WY 2020, where MP 1.6 water temperature was available, and the North Confluence temperature data appeared to have reasonable quality. These years were used to evaluate water temperature model performance.

3.6.3 Lake Ogallala Water Temperature Model

Lake Ogallala is a relatively shallow lake located between the Kingsley Dam and the inlet to the Sutherland Canal (Figure 2). Outflow from the much-larger Lake McConaughy flows into the lake through a hydroelectric project on the Kingsley Dam before entering the canal. The lake is a potentially significant modulator of the temperature of water entering the canal system and could influence ice processes in the canal and siphon. To investigate this hypothesis, and to further evaluate the performance of the water temperature model, we extended the existing model into Lake Ogallala using bathymetric data provided by NPPD (Figure 12). No water temperature data were available at the Kingsley Dam tailrace, so we assumed an outflow temperature of approximately 4°C (39.2°F); however, this value was used as a calibration factor when compared to observed temperatures at MP 1.6. In the absence of flow data from Kingsley Dam, measured flows at MP 1.6 were applied to the upstream end of Lake Ogallala, which may introduce some lag issues during significant flow changes.

Figure 12. Lake Ogallala water temperature model cross sections and extents leading into the Sutherland Supply Canal.

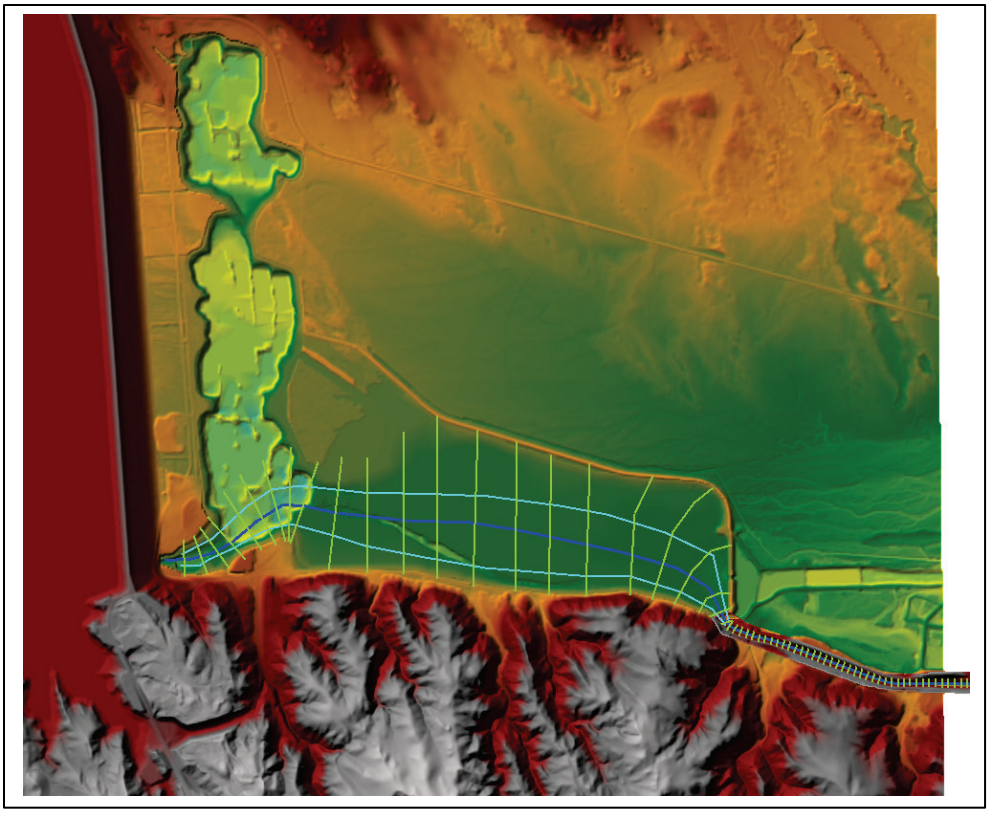

3.7 Potential Frazil Ice Formation in Siphon

The melting point between liquid water and ice is a function of pressure and temperature (Chang 1996). Previous studies have shown that frazil ice formation in conduits can be a significant issue due to depression of the melting point in pressured flow (Ettema et al. 2009). When ice-laden water enters an inverted siphon and becomes pressurized, the depressed freezing point of water can cause the ice to melt, taking up latent heat in the process and supercooling the water. Depending on the ice concentration entering the siphon and the pressure in the conduit, a portion or all the ice may melt while passing through. When the water rises and pressure is reduced, as it does to emerge from the siphon, the supercooled water can refreeze, producing frazil ice with the potential to block the outlet.

The relationship between the freezing temperature and water pressure is nonlinear over the range of 0–200 MPa. However, for relatively small increases above atmospheric pressure (i.e., less than 1 MPa), a linear

approximation of −0.074 °C/MPa is sufficient to estimate the freezing point depression (Ettema et al. 2009).

Absent heat loss through the conduit walls, any actual water cooling towards the temperature depression is caused by melting ice. The relationship between the maximum amount of cooling and ice concentration in the water is linear and can be expressed as

$$\Delta T_{max} = \mathrm{C_{ice}}\left(\frac{\rho_{\mathrm{ice}}\mathrm{L_{ice}}}{\mathrm{C_{p_w}}\rho_{\mathrm{w}}}\right), \quad (1)$$

where

C_{ice} = the concentration of ice (m^3/m^3),
ρ_{ice} = the density of ice (kg/m^3),
ρ_w = the density of water (kg/m^3),
L_{ice} = the latent heat of fusion of ice (J/kg),
C_{p_w} = the specific heat of water (J/Kg-°K), and
ΔT_{max} = the maximum depression in the freezing temperature.

When the ice concentration entering the siphon is just less than that necessary to cool the water to the pressure-based depression of the freezing point, all the ice can melt while transiting the conduit. In this case, the potential for the siphon to be blocked is actually elevated according to Ettema et al. (2009) because there are only a small number of nucleation sites for ice to form as the water depressurizes. The formation of ice in the depressurized, now supercooled, and ice-free water can happen more spontaneously at the exit of the siphon where seed crystals are available to form nucleation sites and water velocities may be lower.

We estimated the expected freezing temperature depression based on the geometry of the Paxton Siphon. This analysis was performed external to the water temperature model using the siphon invert elevations and assuming constant flow velocity through the siphon.

3.8 Forecasting Tool for Ice Formation Potential

A simple forecasting tool was developed to help operations staff to interpret weather forecast data as they relate to potential frazil ice formation. The tool calculates the heat fluxes at the surface of a hypothetical control volume of water. The calculations for heat fluxes used

in this model are based on the same formulations used in the HEC-RAS WQM (Brunner 2016) with some minor modifications.

3.8.1 Heat Flux Calculations

The net heat flux, q_{net} (watts/meters^2) is computed from the sum of five other heat-flux components:

$$q_{net} = q_{sw} + q_{atm} - q_b + q_h + q_l, \quad (2)$$

where

q_{sw} = downwelling shortwave radiation from solar input,
q_{atm} = downwelling longwave radiation from the atmosphere,
q_b = upwelling longwave radiation from the water body,
q_h = the sensible heat flux from air to water, and
q_l = latent heat.

Equation (2) assumes that the surface of the water is unobstructed. Once an ice cover is in place, this assumption is no longer valid, and the model will produce inaccurate results. The model is useful in the periods leading up to ice formation when the water body is open and heat fluxes from ice production are insignificant. These conditions are quite typical prior to periods of frazil ice production when an ice cover has not yet formed.

3.8.1.1 Downwelling Shortwave Radiation

The shortwave radiation from the sun is calculated using the Python library *pvlib* (Holmgren et al. 2018) and is a function of latitude, longitude, elevation, and date. The theoretical clear sky global horizontal irradiance (which is the sum of direct normal and diffuse irradiance on a horizontal plane) is calculated using *pvlib* on an hourly time-step through the forecast period. The theoretical clear-sky value is modified by the amount of cloud cover that will intercept the shortwave radiation:

$$q_{sw} = q_{ghi}(1 - R)(1 - 0.65Cl^2), \quad (3)$$

where

q_{ghi} = the global horizontal irradiance (W/m^2),
R = the reflectivity of the water surface, assumed to be 0.15, and
Cl = the fraction of the sky covered with clouds.

The reflectivity in Equation (3) is assumed to be within the range reported by Maidment et al. (1993) for water.

3.8.1.2 Downwelling Longwave Radiation

The atmosphere emits longwave radiation that is absorbed by water. The atmospheric downwelling radiation is calculated as follows:

$$q_{atm} = \varepsilon_{air} \sigma T_{air}^4, \tag{4}$$

where

ε_{air} = the emissivity of air (unitless),
σ = the Stefan-Boltzmann constant (W/m²·K⁴), and
T_{air} = the air temperature (K).

The emissivity of air was calculated using an empirical formula from Zhang and Johnson (2016):

$$\varepsilon_{air} = 0.937 \times 10^{-5}(1 + 0.17Cl^2)T_{air}^2. \tag{5}$$

3.8.1.3 Upwelling Longwave Radiation

The water body itself emits heat, which is lost in the form of longwave radiation upwards into the atmosphere. The equation for upwelling longwave radiation from the water is similar to the atmospheric downwelling equation:

$$q_b = \varepsilon_{water} \sigma T_{water}^4, \tag{6}$$

where

ε_{water} = the emissivity of water (unitless) and
T_{water} = the water temperature (K).

In Equation (6), the emissivity of water is assumed to be 0.97 for all simulations (Brunner 2016).

3.8.1.4 Sensible Heat

Heat is gained or lost by the water body from or to the air above it. Warm air above cooler water will tend to warm the water while frigid air,

particularly air with a temperature below the freezing point of water, will cool the water body. The sensible heat is calculated using a simplified version of the method in HEC-RAS WQM:

$$q_h = c_p \rho_w (T_{air} - T_{water}) f(U), \quad (7)$$

where

c_p = the specific heat of air (J/kg-K),
ρ_w = the density of water (kg/m^3), and
$f(U)$ = the wind function (m/s).

The wind function in Equation (7) is an empirical relationship like HEC-RAS WQM uses and scales the windspeed. The windspeed equation is

$$f(U) = R(a + bU^c), \quad (8)$$

where

R = the Richardson Number (unitless),
a, b, and c = calibration coefficients (unitless), and
U = the windspeed (m/s).

The Richardson Number in Equation (8) describes the stability of the atmosphere and was set to 1, which assumes the atmosphere is neutral (Brunner 2016). We set a and b equal to 10^{-6} and c equal to 1, which are the default values in the HEC-RAS WQM and consistent with the initial values in Brunner (2016).

3.8.1.5 Latent Heat

The water body may gain or lose heat from condensation or evaporation of water at the surface. Latent heat refers to the change in energy during a phase change. Latent heat released during the transition from liquid water to solid ice is very important in modulating the rate of ice formation. However, this simplified model considers only the latent heat exchange due to the phase change of liquid water to water vapor:

$$q_l = \frac{0.622}{P} L \rho_w (es - ea) f(U), \quad (9)$$

where

P = the air pressure (mb),
L = the latent heat of vaporization (J/kg),
es = the saturated vapor pressure at the water surface (mb), and
ea = the vapor pressure of the air mass above the water (mb).

An empirical equation from Zhang and Johnson (2016) was used for the saturated vapor pressure at the water temperature shown in Equation (9). The saturated vapor pressure equation is a function of water temperature; however, it is too cumbersome to repeat here, and the reader is referred to the source document for more precise details.

The actual vapor pressure of the air is calculated from the dew point (https://www.weather.gov/media/epz/wxcalc/vaporPressure.pdf):

$$ea = 6.11 \cdot 10^{\frac{7.5T_{dew}}{237.3+T_{dew}}}, \quad (10)$$

where T_{dew} is the dew point temperature in Equation (10).

3.8.2 Heat Flux Forecasts

Forecasted heat fluxes are based on the following data from the National Weather Service (NWS) hourly tabular forecast product (NWS, "National Weather Service," n.d.):

- air temperature (degrees Fahrenheit, converted to Celsius)
- dewpoint (degrees Fahrenheit, converted to Celsius)
- surface wind (mph converted to m/s)
- sky cover (%)

Upon execution, the tool requests the most current forecast table at a specified latitude and longitude from the NWS server. The table provides hourly forecast data for each of the next 156 hr in the forecast period.

The model calculates each of the individual heat flux components and sums them to find the net heat flux for a water surface at the user-specified geographic location.

3.8.3 Cooling Rate Forecast

The rate that water cools, particularly as it crosses the freezing point, is known to strongly influence the production rate and overall volume of

frazil ice produced (Ashton 1983; Daly 1984; Ye et al. 2004). Frazil ice production has been observed occurring over an estimated range of cooling rates between -1.29×10^{-3} and -5.02×10^{-2} °C/min (Boyd et al. 2022). Forecasted cooling rates can be compared to this range to predict the likelihood and severity of frazil production.

The user must provide the *characteristic depth*, D, of the control volume, which has a unit surface area. The model assumes that the control volume is fully mixed (i.e., absent the effects of thermal stratification like that which occurs on lakes and ponds). The net heat flux is applied to the control volume and the cooling rate is calculated as follows:

$$\frac{dT}{dt} = \frac{q_{net}}{\rho_w c_{pw} D}, \tag{11}$$

where c_{pw} is the specific heat of water (J/kg).

A cooling rate of the control volume of water is calculated for each hour of the forecast period. When the net heat flux is positive, the cooling rate will be positive as well, indicating that the control volume is warming in response to the added heat. Conversely, a negative net heat flux results in negative cooling rates and cooling of the control volume.

3.8.4 Water Temperature Trace Forecast

If the initial water temperature of the control volume is known, or otherwise is specified, the temperature of the control volume can be forecasted using the cooling rate. In this simplified approach, the water temperature is initialized at a user-specified temperature, and the forecast temperature is calculated by cumulatively adding the forecasted cooling rate for each time-step. This yields a forecasted temperature time series starting at each time-step of the simulation. The approach is approximate because, for simplicity, the cooling rates that are applied to the control volume are calculated with the specified initial temperature, not the calculated values for each time-step. This will affect the calculations of several of the heat fluxes (upwelling longwave, sensible heat, and latent heat). When water temperatures fluctuate in a narrow band of just a few degrees above freezing, the effects of this simplification are likely to be minor, but caution should be used when the results show large temperature variations.

The temperature traces in this method are meant to provide qualitative estimates of the future temperature trends of the control volume. It is not meant to be a substitute for a more quantitative water temperature model (i.e., HEC-RAS WQM) that provides more robust accounting of the energy balance and includes the effects of hydrodynamics.

3.8.5 Graphical User Interface (GUI)

A graphical user interface (GUI) front end (Figure 13) was written using the Python library *Streamlit* (streamlit.io) to control the utilities that compute the heat flux forecast data. The GUI runs in a web browser and allows the user to specify the location of the forecast via latitude and longitude (within the United States) and the characteristic depth of the water. The GUI also allows a user to make forecast requests and generate plots of the results without having to execute the model code at the command line. The user does not need to specify the elevation, which is needed for the solar heat flux calculation because the tool makes a call to a public API at opentopodata.org, which extracts the elevation from the US Geological Survey $^{1}/_{3}$ arcsecond digital elevation model (USGS 2017) at the specified latitude and longitude. The tool can be run locally or can be deployed on a web server for more universal access.

Figure 13. Graphical user interface (GUI) for the heat flux forecast tool.

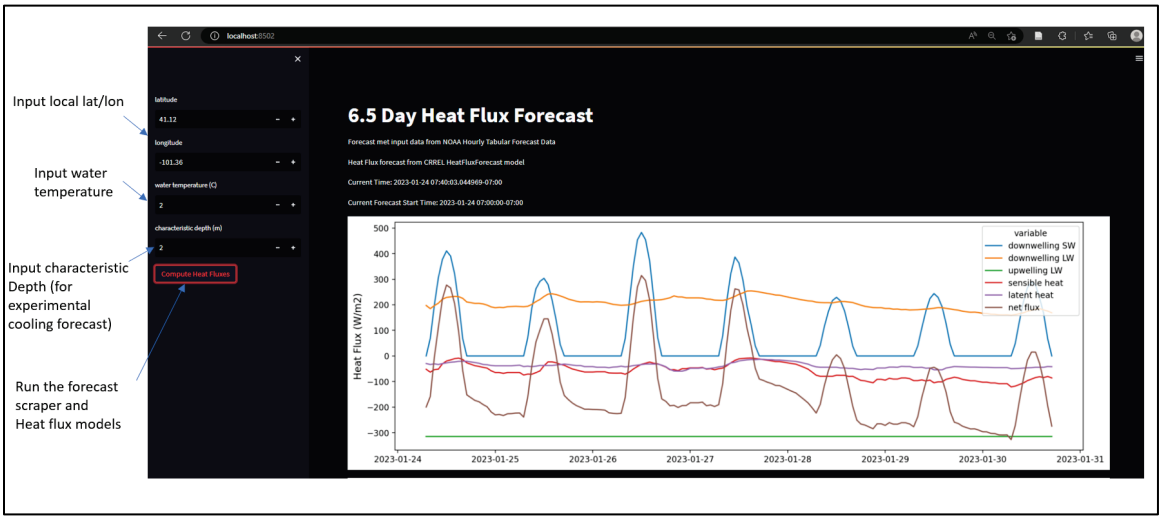

4 Results

4.1 Summary of Annual Ice Events

Based on examination of the stage records available for the supply canal, we found a total of 10 ice-affected stages at the inlet to the siphon during the period 2011–2022. This averages to approximately one ice event per year with the standard deviation slightly over one event. The total number of ice events based on stage records for the supply canal (including the siphon) was 15 during the same 2011–2022 period. This results in just over one ice-affected stage event per year with a similar standard deviation. The annual data are summarized in Figure 14. We did not identify any ice-affected stage events for WY 2006–2010. Due to some stage measurement gaps during the WY 2006–2010 period, we did not include those in the calculated ice-event annual averages.

The data used for our summary are limited in duration, which adds uncertainty to how well the average ice-affected stage events we determine really represent the long-term average. However, it should be expected that annually at least one event will happen with as many as four to five total events possible in a winter season.

Figure 14. Summary of annual ice-affected stage events for the Sutherland Canal based on NPPD gage records from WY 2011 to 2022.

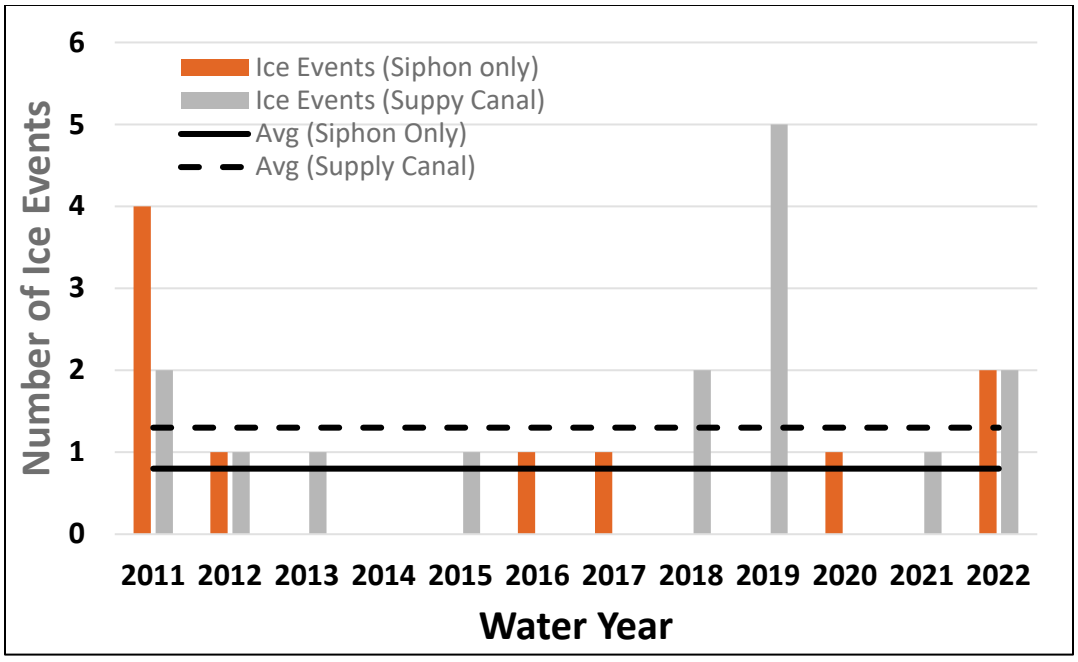

4.2 Hydraulic Modeling

Channel roughness values were adjusted from the original value of 0.0220 used for the entire canal to calibrate to measured stages. Through an iterative process, roughness values corresponding to channel-lining properties were selected by minimizing the difference between the modeled and observed data at stage gages for each year. These yearly values are shown in Table 4 and are grouped by the HEC-RAS model stations associated with the lined and unlined sections of the canal. Model runs in 2019 did not converge on a set of roughness factors due to model instability, so that year was omitted.

Table 4. Yearly and final calibrated Manning's *n* values.

	90600 to 71300	71300 to 60800	60800 to 6900	6900 to 100
	Unlined	Lined	Unlined	Lined
Original	0.0220	0.0220	0.0220	0.0220
2018	0.0238	0.0139	0.0198	0.0077
2019	n/a (unstable)			
2020	0.0286	0.0143	0.0242	0.0110
2021	0.0220	0.0132	0.0198	0.0088
2022	0.0220	0.0132	0.0198	0.0110
Final	0.0220	0.0132	0.0198	0.0099

Table 5 provides a comparison of the original and final roughness values. The final parameters (which are based on the average of the 2021 and 2022 models) were applied to the model alongside the original and observed stages for the January 2022 event, as shown in Figure 15. The calibrated model had better overall error statistics than the original model, and the agreement with observations improved in some reaches, but not in others. Prior to the flow blockage on 6 January, the final winter calibrated HEC-RAS model matched closely to the measured stages compared to the original calibration. The only exception was at MP 5.6, which is a lined section of the canal and upstream of the flume bridge (Figure 2).

Table 5. Comparison of original and final Manning's *n* values by location.

	Root Mean Square		Percent Error		Nash-Sutcliffe	
	Original	Final	Original	Final	Original	Final
90600	0.316	0.595	−0.004%	0.010%	0.980	0.929
69650	0.960	0.558	−0.030%	0.014%	0.807	0.935
62260	0.532	0.431	−0.013%	−0.010%	0.930	0.954
61800	1.153	0.728	−0.034%	−0.015%	0.706	0.883
34528	0.532	1.092	0.012%	0.031%	0.927	0.693
7960	1.364	0.754	−0.043%	−0.015%	0.423	0.824
100	0.496	0.498	−0.006%	−0.006%	0.975	0.974
Average	0.765	0.665	-0.017%	0.001%	0.821	0.885

Figure 15. Calibrated (*solid*), original (*dashed*), and observed (*dotted*) stages during the January 2022 event.

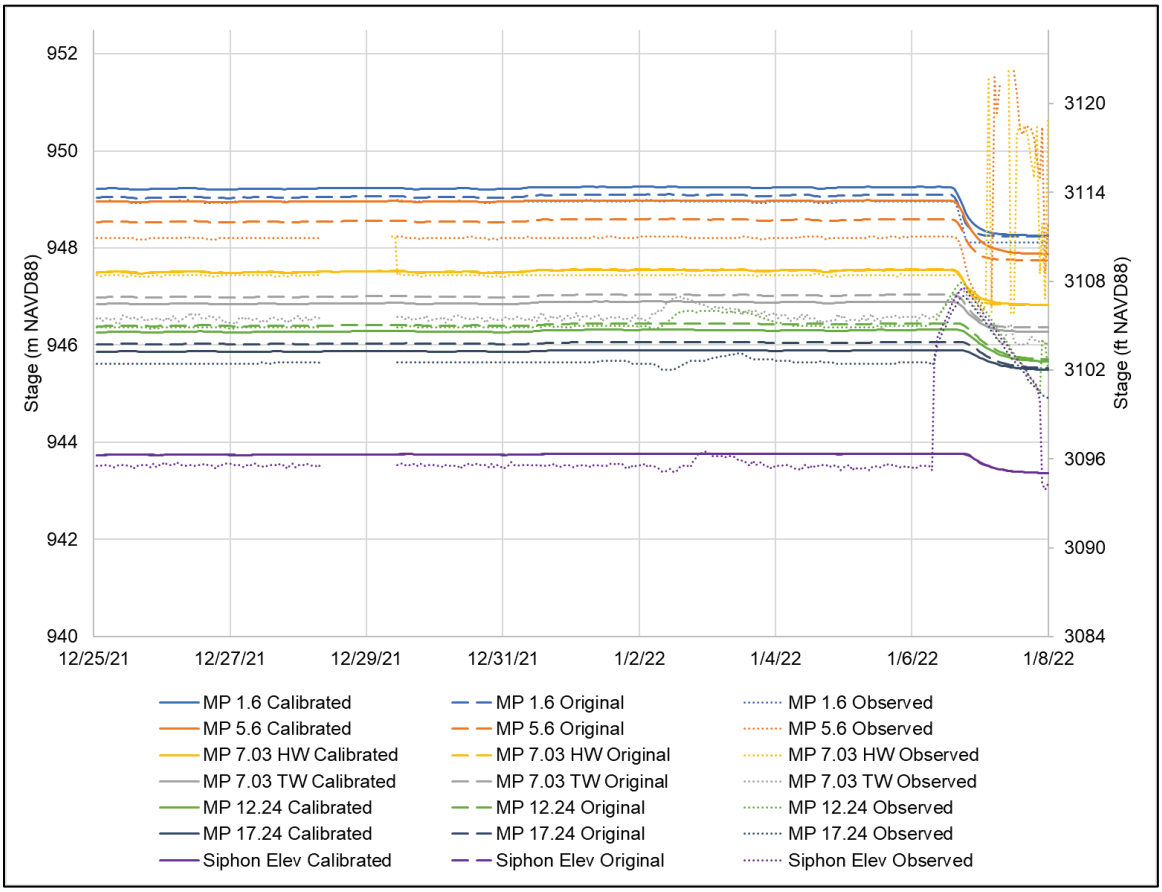

4.3 Water Temperature Modeling

Heat flux components, net heat flux, and simulated water temperatures at each cross section were modeled in the Sutherland Canal. An example of 9 days of water temperature model results is shown in Figure 16. The results are based on the meteorological inputs shown in Figure 11 and the observed water temperature at MP 1.6, which is also shown in Figure 16.

In the wintertime, the net heat flux follows a diurnal pattern with the most negative periods occurring at night when solar radiation input is absent. Negative departures in sensible heat tend to be the strongest drivers of unusually high periods of net heat loss, which is caused by low temperatures and winds.

Figure 16. Water-temperature model results for December 2021 through January 2022.

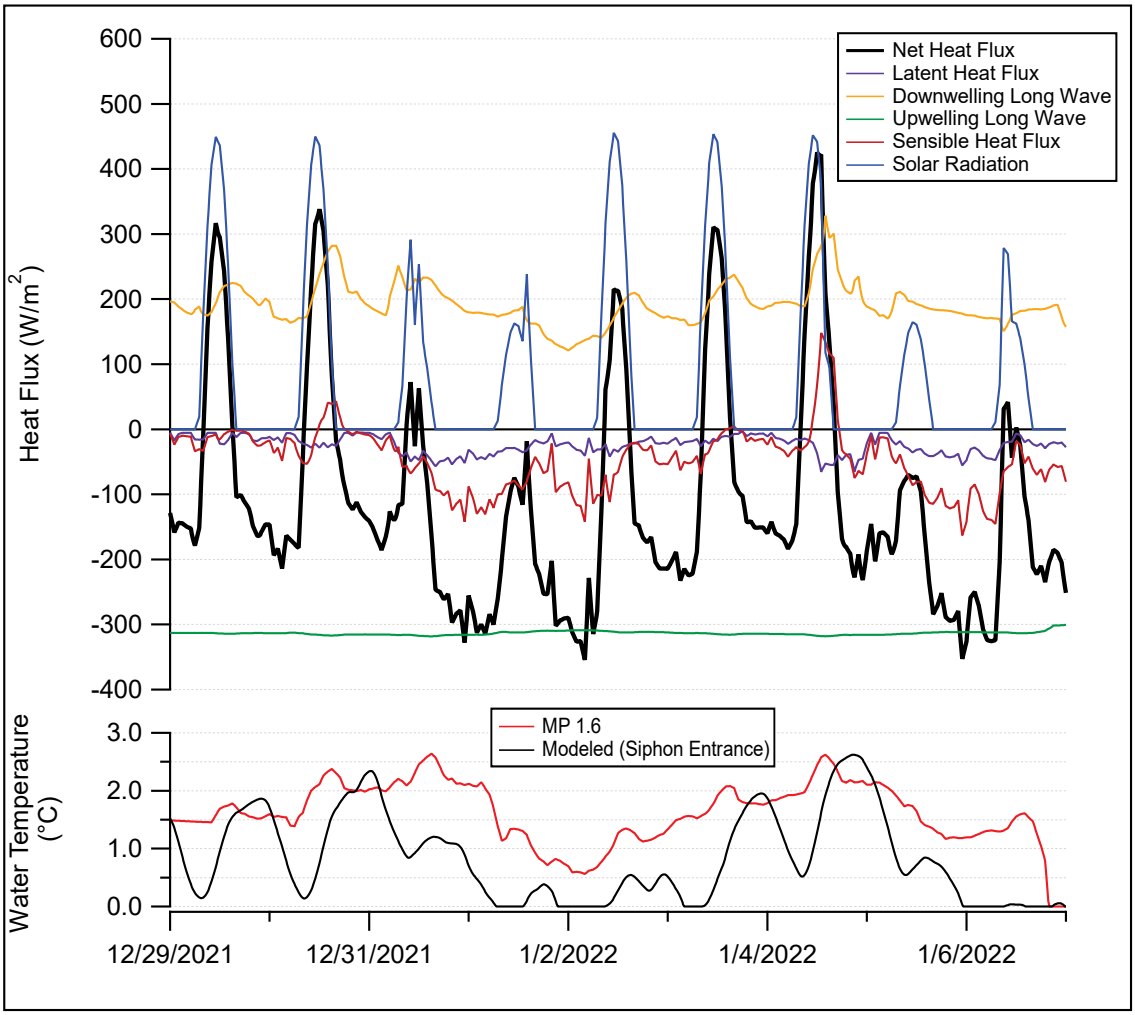

4.3.1 Model Calibration and Error

The simulated water temperatures at the downstream end of the water temperature model (siphon entrance) were compared with observed daily average temperatures at the North Confluence. The period 15–31 December was chosen as the reference period to ideally compare only ice-free periods that still had temperatures near the freezing point. There were 5 yr where temperature data at MP 1.6 and the North Confluence were available in the reference period. Only 2 yr were directly compared because they had the most complete and least noisy observed temperature time series at the North Confluence. The temperature data at MP 1.6 appear to have a systematic error in WY 2013, so the results from that year were not included. Plots of the modeled and observed temperatures are included in Appendix A.

Adjustments to the wind-function coefficients (Equation 8) were made to calibrate the model. The final wind-function values were unity for all but the exponential coefficient *c*, which produced the best results at a value of 1.4. The error results are shown in Table 6 and demonstrate that the water temperature model has an accuracy of approximately 0.5°C, and we know from inspection of the results that it tends to overestimate water temperature.

Table 6. Error summary of water temperature model between MP 1.6 and the North Confluence, 15–31 December.

Year	RMSE* (°C)	MAE** (°C)
2020	0.50	0.39
2019	0.52	0.38
Average	0.51	0.39

*root mean square error
**mean absolute error

A similar comparison between modeled and observed temperatures was conducted with results from the extended Lake Ogallala temperature model. An example of the water temperature results is shown in Figure 17. During ice-free periods, the model simulates temperature with reasonable accuracy, including a precipitous drop in temperature on 27 December 2018 that was largely driven by strong winds enhancing sensible heat transfer. Once an ice cover forms on the lake (identified with PlanetScope imagery [Planet Developers 2023]), the model performance suffers significantly, with the modeled temperatures estimated higher than those

observed, likely due to overestimation of solar radiation that makes it to the ice-covered water.

Figure 17. Example temperature results from water temperature model, simulating temperature change between Kingsley Dam and MP 1.6.

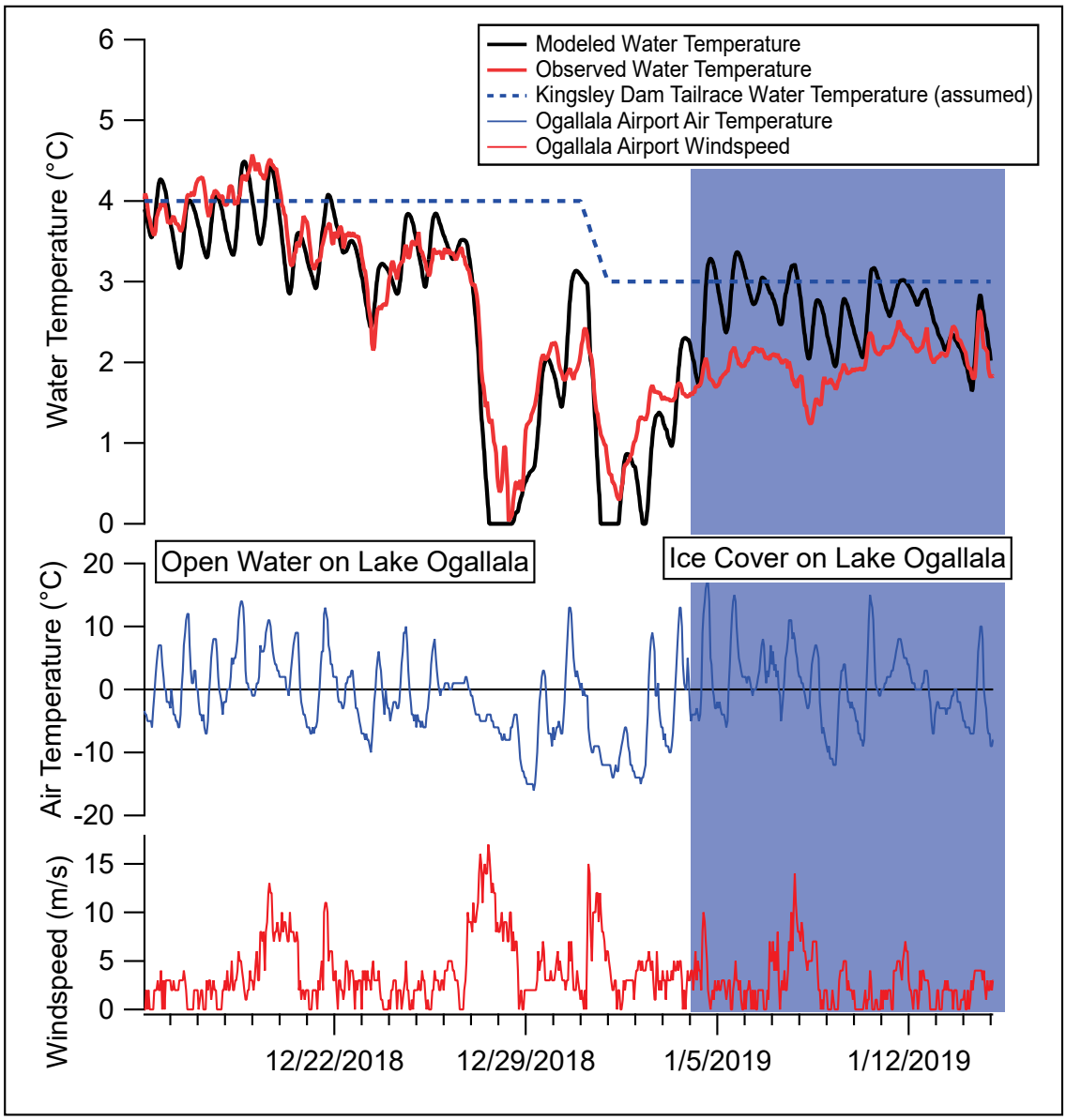

The accuracy of the extended Lake Ogallala model was evaluated over the period 15–31 December for 6 yr (Table 7) when open water was more likely. The wind function coefficients were the same as those used in the model of the full canal. The model had an accuracy of approximately 0.6°C and tended to overpredict water temperatures (i.e., underpredict potential for freezing).

Table 7. Error summary of water temperature model between Kingsley Dam and MP 1.6 15 December–31 December.

Year	RMSE (°C)	MAE (°C)
2022	0.62	0.50
2020	0.46	0.35
2019	0.43	0.32
2018	0.81	0.67
2017	0.58	0.48
2016	0.55	0.43
Average	**0.57**	**0.46**

We found that a nearly complete ice cover was present a few days before the cold weather in January 2022, which would indicate frazil ice traveling from the lake into the Sutherland Canal would be minimal.

4.3.2 Energy and Temperature Results

The calibrated temperature model was used to simulate heat fluxes and water temperatures for WYs 2011–2022, with WYs 2006–2010, 2014, and 2021 omitted due to insufficient data or data quality concerns.

Modeled water temperature for the siphon entrance is shown in Figure 18. The results provide an indication of when ice formation occurred both spatially along the canal and temporally during the cold-weather event. While water temperatures reaching the freezing point likely did begin to produce ice, the rate of ice formation in some cases was probably slow enough to not create much of an influence on hydraulics. As we are particularly interested in events where significant frazil ice volumes were produced, a high rate of cooling is likely a strong indicator. The modeled heat flux for each year of the simulation period is shown in Figure 19 and demonstrates the range of negative heat fluxes regularly extends beyond −300 W/m^2 going as low as −450 W/m^2 in February 2011.

Figure 18. Observed model input temperature (*red*) and HEC-RAS modeled temperatures (*blue*).

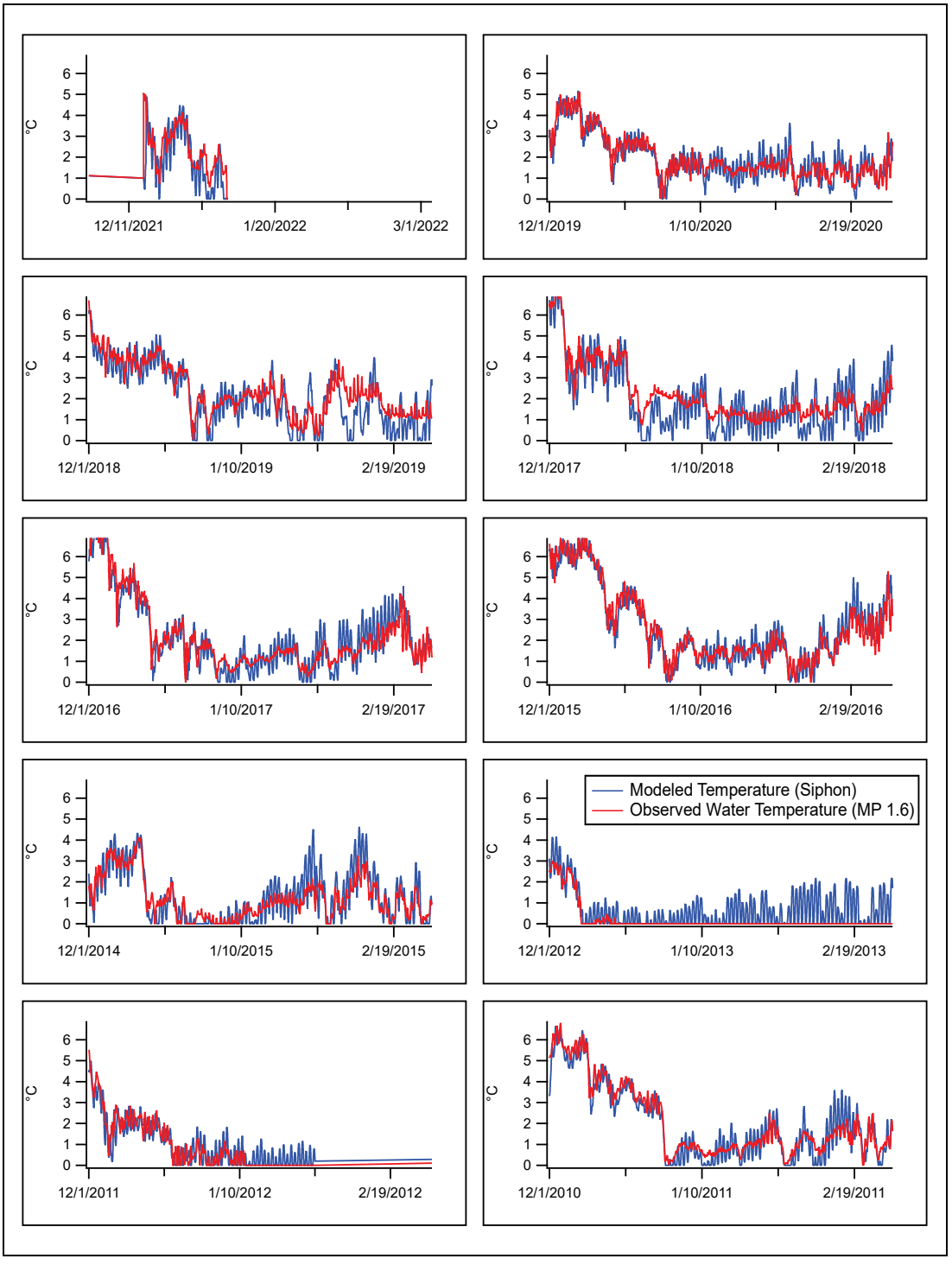

Figure 19. Simulated net heat fluxes for WY 2011–2022, WY 2021, and WY 2014 omitted due to lack of observed water temperature data.

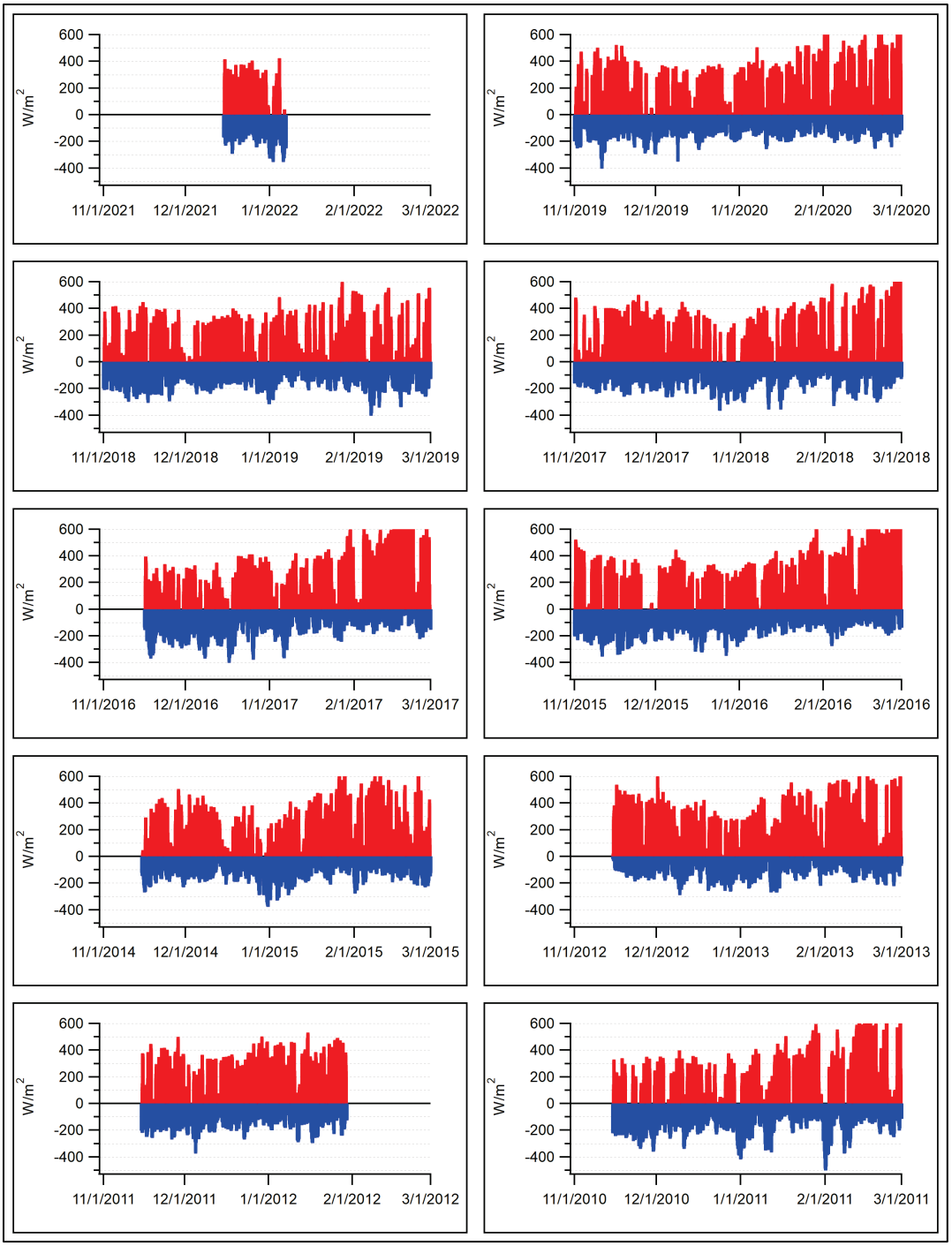

We reviewed the observed stage at gages along the canal for each event where the temperature model calculated a sustained heat flux of −350 W/m² or less (more negative). While fewer than two events exceeded this threshold, we found a clear pattern of anomalous stages during some of those events indicating the effects of ice. When water temperatures were approximately 3°C (37.4°F) or colder prior to the event, stages tended to rise likely due to increased friction or reduced conveyance from ice that formed in the channel (Figure 20). When water temperatures of 4°C–5°C (39.2°F–41°F) preceded the event, the water temperature did not reach the freezing point according to the model results, and there were no anomalies in the stage records indicating ice did not form (Figure 21).

Figure 20. Siphon icing event in January 2011.

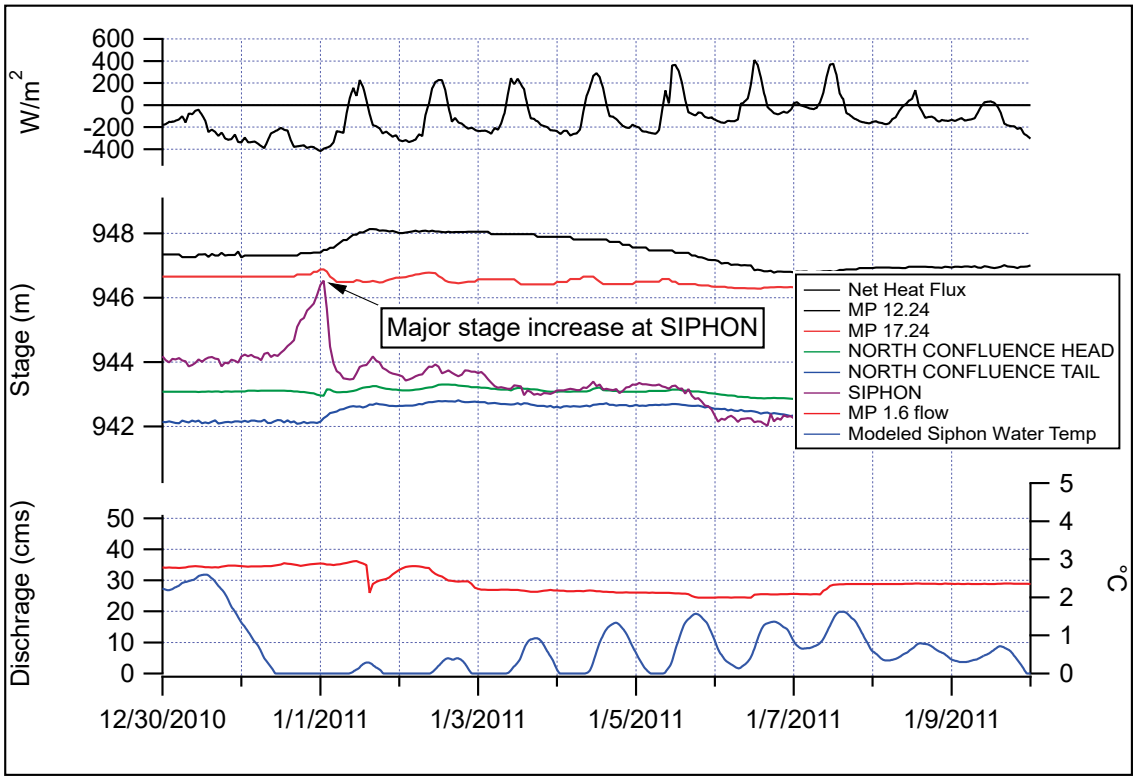

There was not a strong correlation between flow rate and ice effects, but the population is small, and it is difficult to generalize based on the limited set of events. Flow in the canal was lower during the 2022 event (total flow of approximately 12 cms [424 cfs]) than in almost all the other stage anomaly events; however, higher flow rates did not prevent icing. In 2012 and 2017, there were clear icing events when flows were approximately 30 cms (1,059 cfs), and in 2011 there were dramatic increases in stage upstream of the siphon at similar flow rates (Figure 20). The hydraulic behavior at the

siphon entrance experiences a transition between supercritical and subcritical flow at approximately 34 cms (1,200 cfs) (Edward Dekleva, personal communication, 22 March 2023). When the flow is lower than 34 cms (1,200 cfs) and is supercritical at the entrance, obstructions from ice in the siphon may not affect stage at the siphon entrance, and those events may go undetected. Conversely, when the flow is higher than 34 cms (1,200 cfs), and is subcritical at the entrance, obstructions downstream may have a more muted effect on stage. The most significant stage changes at the siphon entrance are likely to occur when the flow is at approximately 34 cms (1,200 cfs), is supercritical, and the obstruction causes the flow at the entrance to transition to subcritical flow, which may be the case for the 1 January 2011 event depicted in Figure 20.

Figure 21. Negative heat flux of nearly 400 W/m² did not cause ice formation due to initial water temperature of 4°C (39.2°F) at MP 1.6.

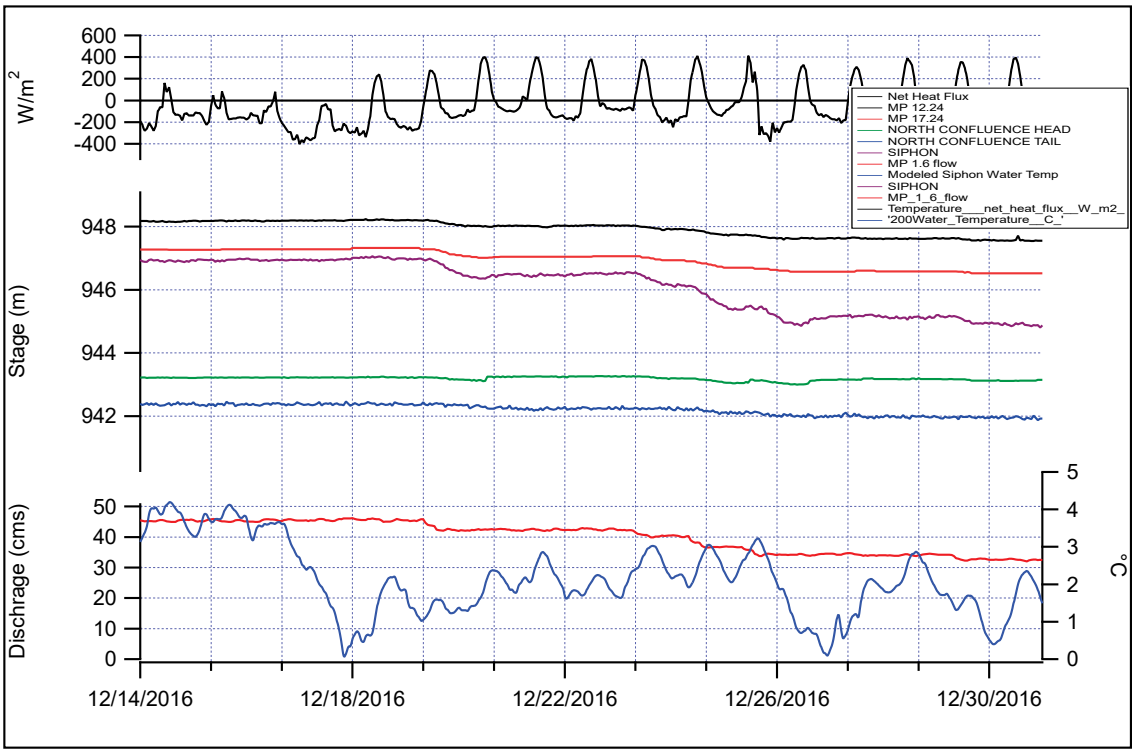

From these results, we can establish an approximate generalization for predicting potentially significant icing events under open-water conditions: when upstream water temperatures are approximately 3°C (37.4°F) or less and estimated heat loss is greater than 350 W/m², ice formation and stage rise are likely. Appendix B shows additional heat flux plots for other years with ice-affected stages.

4.3.3 January 2022 Events

In late December 2021 and into January 2022, there were three events that met the upstream water temperature and heat flux criteria, in the morning of 1 and 2 January and again on 6 January (Figure 22). On all 3 days, the model predicted that water in the canal would reach the freezing temperature, and with modeled heat fluxes on the order of negative 300–350 W/m², ice formation was likely. In the morning of 1 January, the stages rose on the upstream and downstream North Confluence gages, likely due to frazil ice forming in the canal, passing through the siphon, and becoming jammed downstream.

Figure 22. Negative heat flux and evidence of ice-affected flow upstream and downstream of the siphon in January 2022.

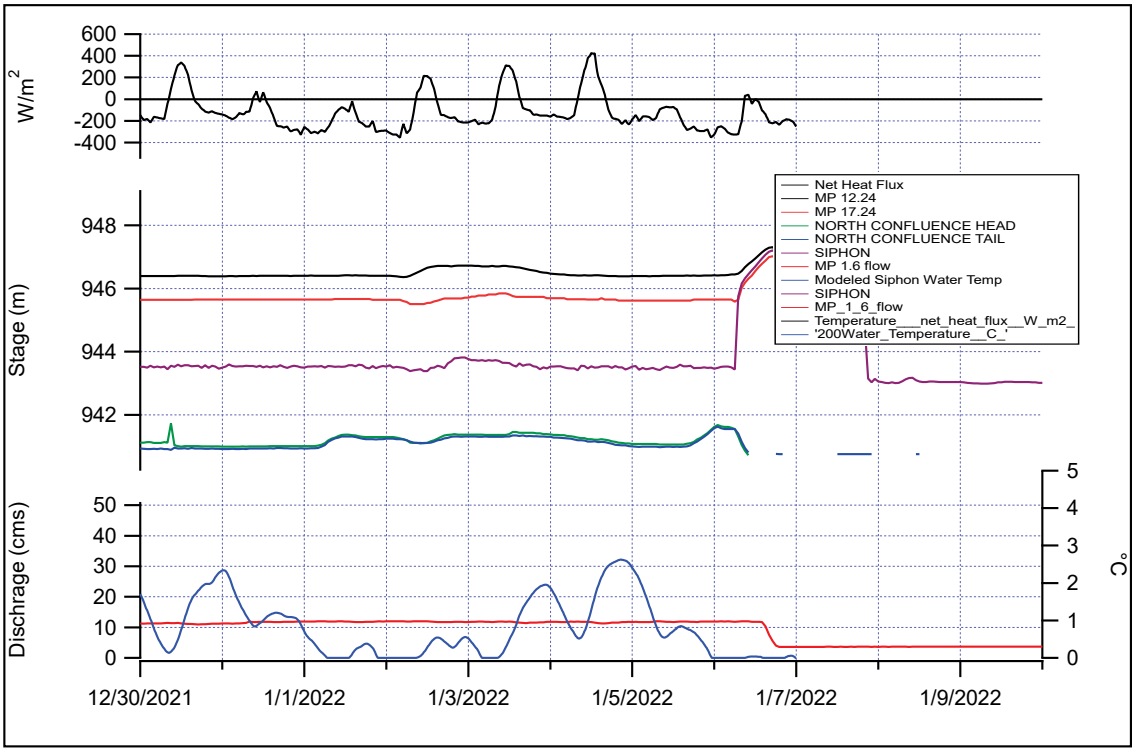

There were no signs of stage changes due to ice formation upstream of the siphon until the second event on 2 January when the stage rose at MP 12.24 and stages fell downstream, which indicates the formation of a frazil jam between MP 12.24 and 17.24. Stages recovered to open-water levels later in the day on 2 January as the net heat flux turned positive, and a subsequent rise in stage at the siphon may have been from frazil ice moving through the system downstream of the siphon. Warmer weather moved in between 3 to 5 January, and the stages relaxed to near their normal open-water levels.

High-resolution satellite imagery was sparse during that period, but a collect on 4 January clearly shows accumulated ice in the canal downstream of the North Confluence check (Figure 23). In the evening of 5 January, temperatures dropped to approximately −20°C (−4°F) with winds of approximately 5 m/s (11.1 mph) creating a heat flux that reached approximately −350 W/m² continuing into the morning of 6 January.

Figure 23. PlanetScope Image from 4 January 2022 showing ice accumulated in bends downstream of siphon in Sutherland Canal. (PlanetScope Imagery acquired 26 January 2023.)

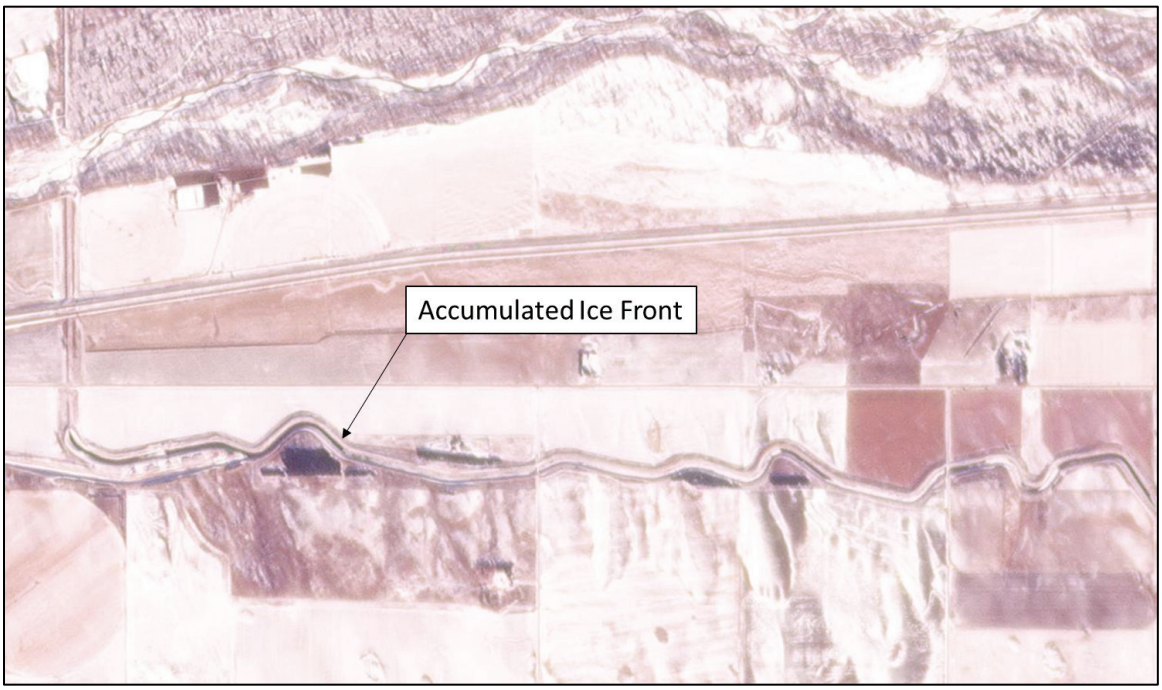

Stages at the North Confluence check began to rise at approximately 15:00 on January 5, which is approximately 9 hr before the model-predicted water temperatures at the siphon would reach the freezing point. This discrepancy is likely partially an artifact of the way the water temperature model calculates solar radiation; the reduction in solar radiation from cloud cover is limited to 65% even with complete coverage (Equation 3). In this study, we used calculated solar radiation based on the earth's position relative to the sun and reduced based on cloud cover reported at OGA. Solar radiation data were available from local personal weather stations but were not used in the model due to length of record and possible issues with topographic shading. However, the locally observed solar radiation from North Platte shows that 5 January had an unusually low amount of incoming solar radiation (Figure 24), less than half of the calculated radiation even after correcting for the reported complete cloud cover at OGA.

When corrected, the net heat flux in the late afternoon of 5 January would be even lower than the modeled results show (Figure 16). The simulated water temperature is approximately 0.5°C (32.9°F), which is within the model error, when the stages begin to rise at the North Confluence check. It is very possible that frazil ice formation did begin to form upstream of the siphon on the ususually dark, cold, and windy afternoon of 5 January.

Figure 24. Modeled solar radiation and observed solar radiation at KNENORTH14 located north of North Platte, Nebraska.

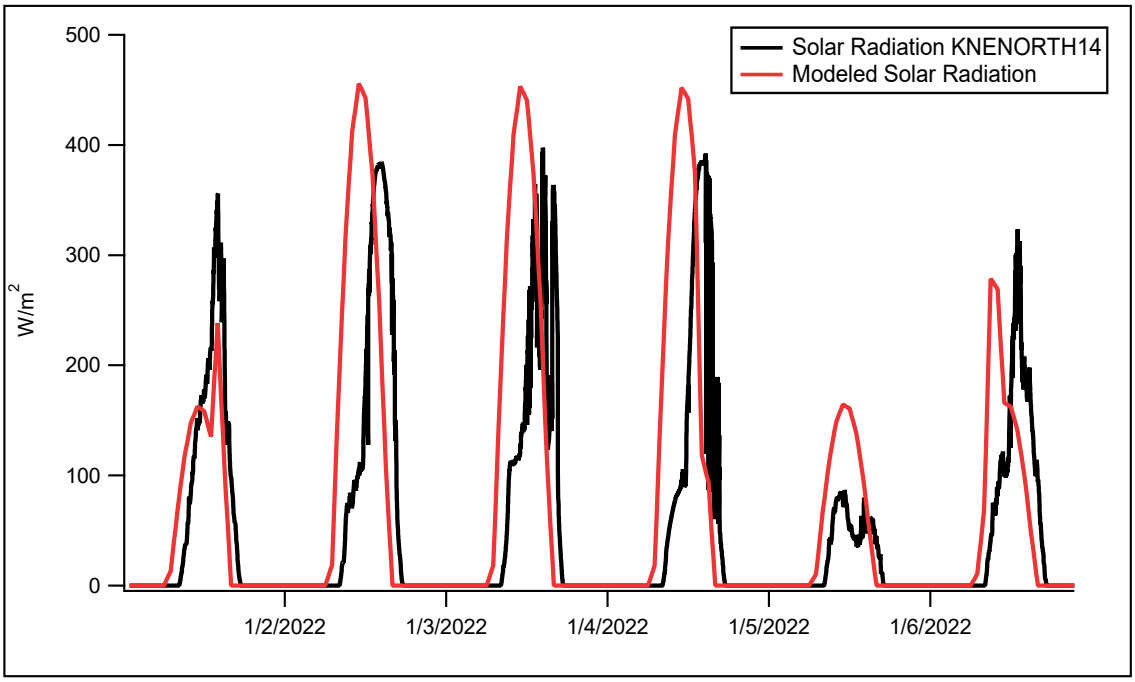

Conditions suitable for frazil ice formation continued through the evening and into the morning of 6 January. Between 22:00 and 23:00 on 5 January, the temperature model shows approximately 13 km (8 miles) of the canal reached the freezing point from the siphon to upstream past MP 12.24 (Figure 25). This likely caused widespread formation of frazil ice along this length before a localized frazil-producing front formed between MP 12.24 and MP 7.03. The nearly simultaneous freezing of a large length of the canal is not unusual with similar patterns having occurred on 1 and 2 January, which both lead to apparent ice accumulation and stage rise at the North Confluence check. As water in the affected channel supercooled and produced frazil, much of the length likely entered a residually cooled state where latent heat released during ice formation balanced with reduced heat loss to the atmosphere due to the ice cover. Much of the subsequent frazil ice formation likely occurred at a localized frazil forming

front in the canal. As discussed earlier, overestimation of solar radiation input may have caused the temperature model to predict slightly delayed frazil ice formation. The gage data suggest that ice accumulation started below the siphon at approximately 15:00.

Figure 25. Modeled temperature zones in the canal upstream of the siphon.

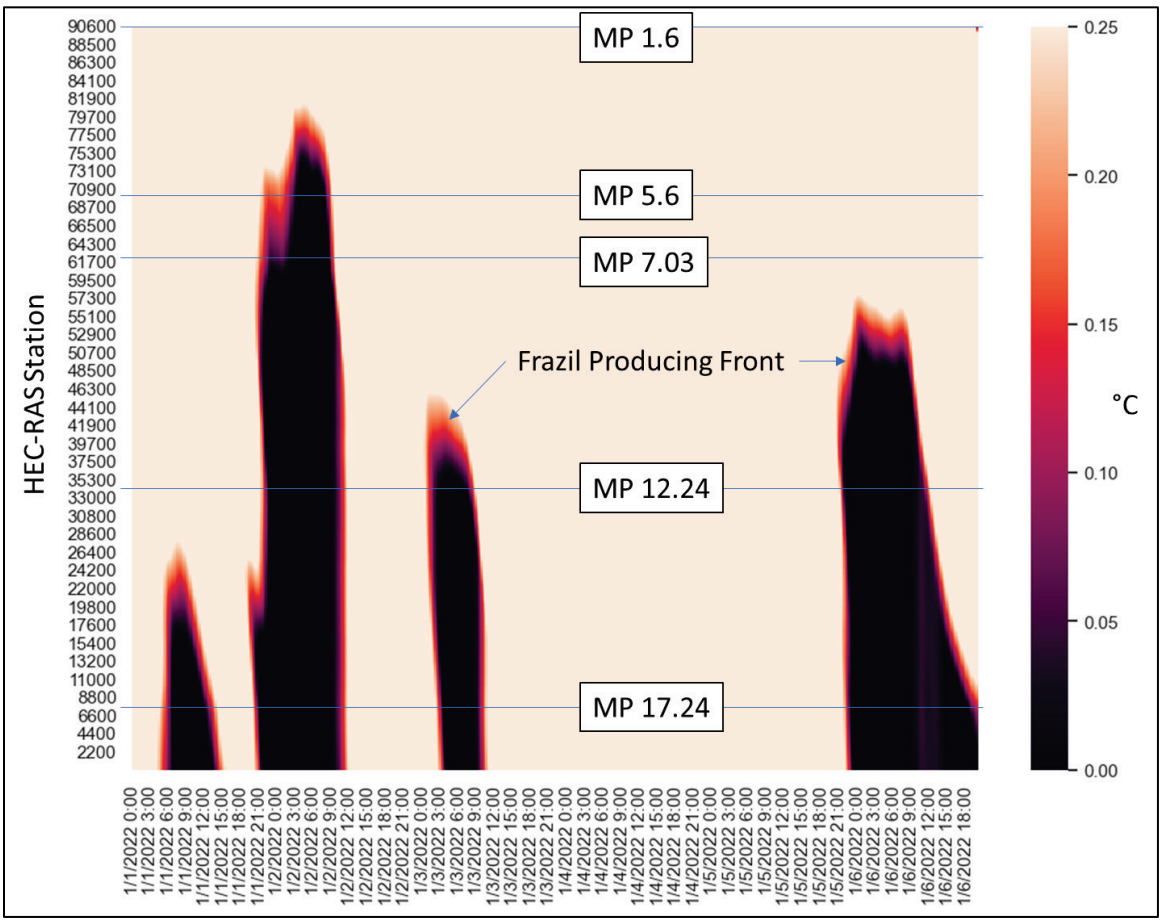

The North Confluence gages continue to rise together until just after 01:00 (Figure 26), likely due to accumulation of frazil ice in the already ice-obstructed channel below the North Confluence check. The frazil ice accumulating at this point was likely formed during the initial cooling of the canal in the afternoon and evening of 5 January. During this period, the stable ice front was likely advancing upstream towards the siphon outlet as arriving frazil ice was arrested. At approximately 01:21, there is a sudden 0.15 m (0.5 ft) spike at the siphon gage, followed approximately 1 min later by a drop in stage at the tailwater of North Confluence check indicating the formation of a frazil jam either in the siphon or more likely in the channel directly upstream of the North Confluence check. After the initial surge, the siphon gage stabilizes at a slightly elevated level,

indicating that the jam remained in place but in a steady state condition with no increases in stage either at the siphon or the North Confluence check. Note that the effects of a potential downstream obstruction were being seen at the siphon gage because at a flowrate of approximately 11 cms (388 cfs), the hydraulic condition at the siphon entrance would be supercritical, indicating the obstruction was significant enough to back flow up through the supercritical section to the gage.

Figure 26. Canal stages during the 6 January 2022 ice-blockage event.

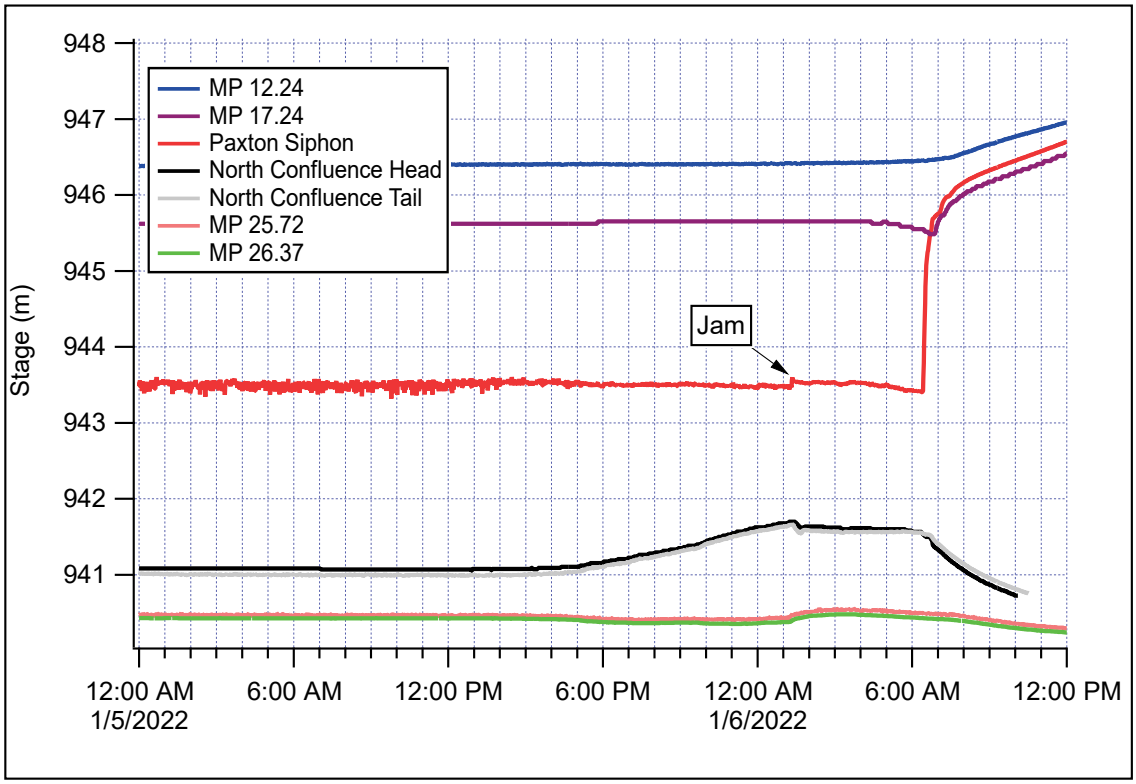

At this point in the event, a stable frazil ice-generating front had likely formed somewhere upstream of MP 12.24, which was producing ice that was then transported downstream. Based on an estimated flow velocity of 0.5 m/s (1.64 ft/s), frazil generated at the front approximately 12.8 km (8 miles) upstream of the siphon would take approximately 8 hr to reach the siphon. Ice-volume concentrations produced at the localized front may have been much higher than the original concentrations formed earlier in the freezing cycle.

At approximately 04:00, a subtle stage rise is observed at the MP 12.24 gage with a coupled stage drop at MP 17.24 indicating the formation of an ice jam between the two (Figure 26). This indicates the flow rate

downstream of MP 17.24 and entering the siphon likely decreased during this period.

While there is insufficient observational data to fully confirm this hypothesis, the available evidence supports the following narrative: frazil formed during an initial period of cooling of 14 km (8.7 miles) of the canal upstream of siphon. This initial frazil ice accumulated downstream of the siphon, building up on ice that was in place from frazil-producing events earlier in the week. This caused an accumulated frazil ice front to advance through the North Confluence check, creating a small jam somewhere near the end of the siphon. Contributing to the jam formation at the North Confluence check was the lack of surface velocity because the check gates were open for flushing of vegetation on the upstream side of the check. Normally, when the check gates are closed and the center weir is the stage control, we would expect some movement of ice past the North Confluence check. Water levels in the system stabilized for the next 3–4 hr while either the initial frazil supply was exhausted or otherwise stalled upstream of MP 17.24. Ice formation at a localized front upstream of MP 12.24 traveled downstream before jamming upstream of MP 17.24 and reducing flow in the channel downstream. At approximately 05:00–06:00 on 6 January, concentrated frazil ice arriving from the frazil ice-producing front (generated approximately 8 hr earlier) encountered the jam upstream of the North Confluence check. The reduced flow rate from upstream jams reduced the velocity in the siphon slightly, and the arriving frazil concentration was high enough to block the siphon such that even with a significant increase in driving head, the obstruction could not be dislodged.

4.4 Potential Frazil Ice Formation in Siphon

Based on the pressure computed for the Paxton Siphon, the risk of frazil ice formation from depressurizing supercooled water within the siphon is very low. The maximum pressure in the Paxton Siphon at the deepest point will depress the melting/freezing point to approximately –0.014°C (31.975°F) (Figure 27). The concentration of frazil ice needed to supercool the water to the depressed freezing point is 2×10^{-4} m^3/m^3 based on Equation (1). If the concentration of frazil ice is just a bit lower than this, all the ice will melt, and ice-free supercooled water would potentially rapidly form and stick to the conduit when depressurizing.

Common frazil concentrations in streams and reservoirs are on the order of 1.6×10^{-3} m^3/m^3 (Ettema et al. 2009), which is an order of magnitude above the concentration required to cool the water to the maximum temperature depression in this case. In addition, based on supercooling rates estimated by the water-temperature modeling, the concentration of frazil ice upstream of the siphon is expected to be much higher than either of these values. This means that while some portion of the frazil ice entering the siphon will likely melt and supercool the water, not all of it will. Frazil flocs will be available throughout the conduit transit to provide nucleation sites for ice to grow, release latent heat, and modulate the supercooling.

It will be difficult to directly quantify how much frazil ice is forming in the siphon without additional temperature monitoring at the entrance and exit with high precision instrumentation.

Figure 27. Potential frazil ice formation within the Paxton Siphon due to melting-point depression associated with increased pressure.

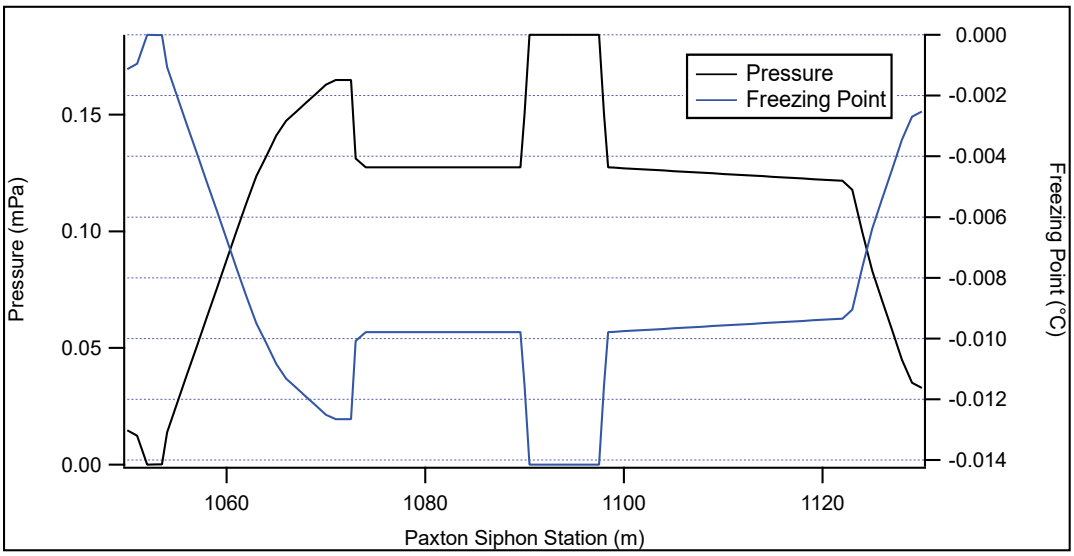

4.5 Forecast Tool Output

The heat flux forecast tool produces forecast data for the next 6.5 days from when the tool is run. The main outputs from the tool are the individual heat flux components and the net heat flux (Figure 28), the calculated cooling rate of water at the characteristic depth (Figure 29), and the calculated water temperature traces from (Figure 30).

Figure 28. An example of the 6.5-day heat flux forecast.

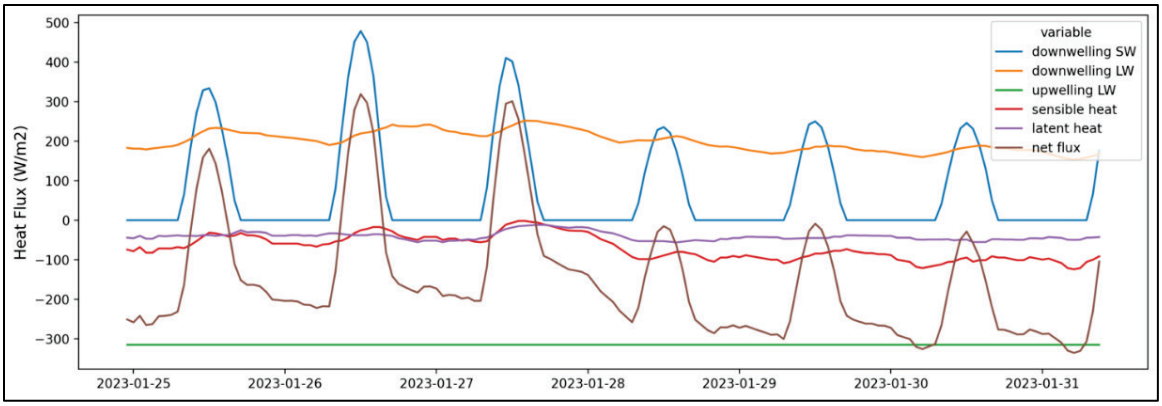

The heat flux forecast can be used to estimate the potential for frazil ice formation in the canal system. As discussed earlier, an apparent threshold of 300–350 W/m² heat loss is an indicator of ice formation based on a review of prior icing events on this system. The heat flux forecast is based only on the location of the estimate and the assumptions discussed in the methods section.

Figure 29. An example of the 6.5-day cooling rate forecast.

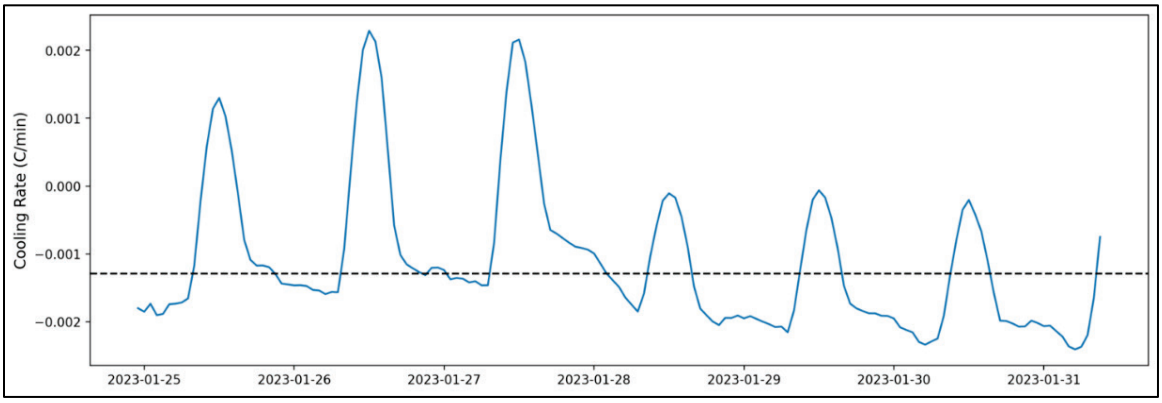

The cooling rate forecast is a more general indicator of the potential for frazil ice generation and is scaled by the user-defined characteristic depth. It is assumed the water column is fully mixed, but the cooling rate will decrease with deeper water with more heat capacity. The *dashed line* in the cooling rate plot is the minimum cooling rate associated with frazil ice generation from Boyd et al. (2022). More negative cooling rates are associated with more frazil generation, though the tool does not attempt to calculate concentration.

Figure 30. An example of the 6.5-day hourly water temperature traces.

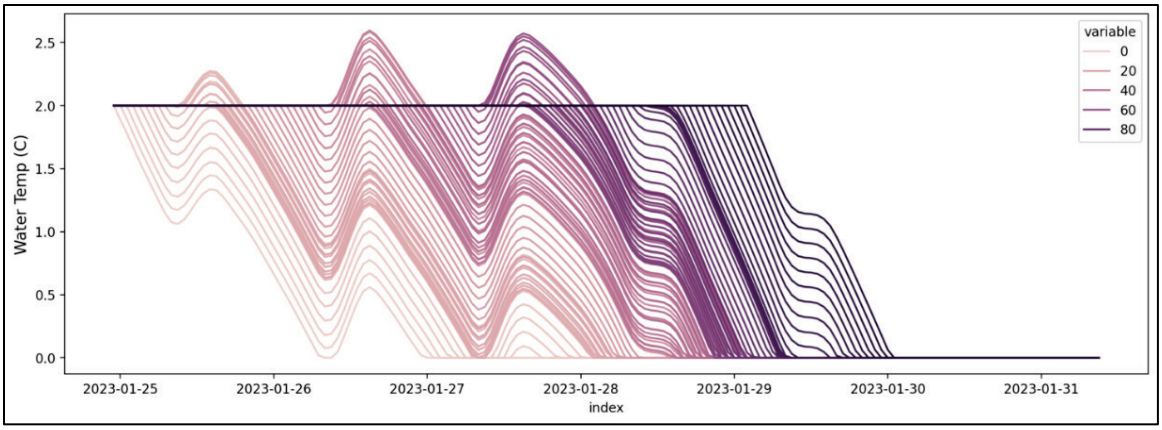

The temperature trace plots provide a basic outline of how the temperature of water in the canal may evolve based on the user-specified characteristic depth, initial water temperature, and the forecast heat flux forecast. This is a major simplification of the water temperature simulation produced by the HEC-RAS WQM but is much easier to estimate on an ongoing basis. The traces do not include any spatial component and extend to the end of the forecast window. A parcel of water starting at the upstream end of the canal would reach the siphon area at a time based on the flow rate, which is likely much shorter than the total calculated temperature trace.

While the temperature traces are quantitative, they should be used only qualitatively because they are based on an uncalibrated model with many simplifying assumptions. The user should use them to identify periods where water temperatures are forecast to rapidly drop to the freezing point within the time window that a parcel would transit the canal system.

The water temperature model in HEC-RAS could also be used in a forecast mode, but this would require generating input boundary conditions based on forecast weather data, anticipated water inflows, and water temperatures at the upstream end of the model.

5 Conclusions and Recommendations

5.1 Conclusions

The frazil ice blockage event for the Paxton Siphon was unique. Given the lack of previous frazil ice blockages in the siphon and lack of record-breaking subfreezing temperatures, the exact combination of conditions is difficult to determine. The air temperatures during early January 2022 were cold but certainly not the most extreme based on the 26 yr of data at OGA. The flow in the Sutherland Canal was lower than average but again not substantially different than recent drought years. The coldest period in the period of record for OGA was when daily average air temperature reached −25°C (−13°F) in mid-February 2021. Based on the stage records, there appears to be ice-affected stage for locations upstream of the siphon but not at the siphon entrance. In addition, no notable ice accumulation occurred in the siphon.

Based on the data observations available to us, there is likely not a single specific environmental variable or water management action that resulted in the flow blockage of the Paxton Siphon. Rather, there was a combination of circumstances that aligned both temporally and spatially on NPPD's Sutherland Canal. In our estimation, the primary contributing factors to the January 2022 event were two consecutive cold weather events (1–2 January and 5–6 January), ice accumulation in the canal downstream of the Paxton Siphon, and reduction of stationary ice cover upstream of the siphon during the relatively warm period on 3–4 January. From our analysis of temperatures in the canal, the frazil ice formation is occurring predominantly in sections upstream of the siphon. It is unlikely the large concentration of frazil ice needed to completely block flow is being generated within the siphon.

From the analysis presented in this report, we can establish an approximate generalization for predicting potentially significant icing events under open-water conditions: when upstream water temperatures are approximately 3°C (37.4°F) or less and estimated heat loss is greater than 350 W/m2, ice formation and stage rise is likely.

To mitigate this type of event in the future, an important step would be to maintain competent ice cover for sections of the canal upstream of MP 17.24. This will reduce the potential for frazil generation and hold back

ice that could otherwise accumulate in the channel downstream of the siphon. In addition, monitoring of water temperature could provide direct information about the potential for frazil ice formation during supercooling periods. Operationally, there may be some actions that warrant further investigation such as increasing flows into the canal or mechanically removing ice from the North Confluence check. However, flow increases would not necessarily reduce the total frazil ice entering the siphon either. While additional flow would take slightly longer to become super cooled due to *thermal mass* of the liquid, in many cases the point in the supply canal where frazil ice formation would initiate would likely only be shifted somewhat downstream, delaying but not preventing ice formation. In addition, at higher flow rates, more water surface would be exposed to frigid air conditions, which could offset the benefits of increasing the thermal mass. The primary advantage of increasing flow would be increased transport capacity of frazil ice through the siphon. However, increasing the flow and transport capacity would increase risk in the event of a complete blockage of the siphon.

5.2 Recommendations

Water temperature measurements are a key data limitation that make modeling frazil ice formation and accumulation in the Sutherland Canal and Paxton Siphon with a process-based hydrodynamic model challenging. Without validation information, we cannot quantify the error associated with these types of models and limits any assessment of how useful the model would be for NPPD. Another data limitation is monitoring for frazil ice concentrations at various locations in the canal. This type of information would increase our ability to relate frazil concentration to changing flow and weather conditions. In addition, estimates of transport capacity through the siphon can be made given the frazil ice concentration and flow velocity in the conduit.

We have several specific recommendations for NPPD to improve monitoring and potentially limit frazil ice formation upstream of the siphon. In addition, we recommend using the modeling and forecast tools developed in this study to help provide general awareness of potential supercooling events that will result in frazil ice formation. Finally, we have listed ideas for future investigations that would reduce the current knowledge gaps related to frazil ice formation in the Sutherland Canal:

- Monitoring
    - Water temperature: Installing additional water temperature sensors would help both for operations during cold-weather events and provide validation of modeling results we will be providing from the water temperature model. A range of water temperature probes are available, but we would recommend installing probes that can measure supercooled water in at least one or two locations upstream of MP17.24. We would also recommend collection of discharge temperature from Kingsley during the cool season (December–March). In addition, additional temperature monitoring using high precision water temperature probes at the entrance and exit of the siphon would help quantify the effects of pressure induced melting of ice and heat exchange through the siphon walls.
    - Frazil ice: Using a Shallow Water Ice Profiling Sonar for monitoring frazil ice concentrations in the supply canal upstream of the siphon could prove to be valuable information. Additional frazil ice monitoring downstream of the siphon is also recommended. This would potentially allow for alarms to be triggered for operations staff. In addition, flow adjustments could be conducted, and ice formation could be monitored, which would provide greater confidence of solutions involving changes in canal discharge. The Cold Regions Research and Engineering Laboratory (CRREL) is currently developing lidar-based instruments for monitoring frazil ice concentration, but the systems are at a research and development stage currently and would not be suitable for operational use until more testing has been conducted.
    - Meteorological Data: Installing an onsite radiometer to measure incoming solar radiation will help get a better understanding between computed and measured solar radiation used in the temperature modeling and would be useful to use directly in the heat flux forecast tool.

- Mitigation and modeling
    - Ice booms: This is likely one of the most effective ways to prevent future ice blockages of the Paxton Siphon. These are relatively low cost and can help promote surface-ice formation on the supply canal upstream of the cut section. This would reduce the reaches

with open-surface water conditions and therefore reduce areas of potential frazil ice formation. These would also reduce the volume of ice entering the siphon and accumulating downstream.
    - Mechanical ice removal: Removing or promoting the movement of ice away from the North Confluence check may be a useful mitigation measure. This would allow frazil ice flowing through siphon to continue moving downstream.

- Modeling and forecasting tools

    - Predicting water temperature: Using the HEC-RAS WQM to predict the timing and location of ice formation could provide useful information for water management and canal patrol personnel. In addition, future modeling efforts could integrate additional data collection locations, which would refine the parameterization of the HEC-RAS WQM.
    - Utilizing the web-based tool CRREL Heat Flux Forecast Tool: Monitoring forecast heat fluxes are a potentially useful method to be prepared for frazil ice generating events.

- Future investigations

    - Test release in canal: The effectiveness of varying discharge in the supply canal is difficult to quantify. There is some evidence from the modeling to suggest that decreasing flow during cold events would reduce the total frazil ice entering into the siphon. However, after water temperature monitoring and frazil ice concentration data are being collected, a test release with a series of incremental discharge changes can be performed during cold-weather events. This would provide information about how frazil ice concentrations vary with discharge. Monitoring above and below the siphon would be most useful since estimates of any deposited frazil within the siphon could be made.

References

Andersson, A., and S. F. Daly. 1992. *Laboratory Investigation of Trash Rack Freezeup by Frazil Ice*. Report No. 92-16. Hanover, NH: US Army Corps of Engineers, Cold Regions Research and Engineering Laboratory.

Ashton, G. D. 1983. "Frazil Ice." *Theory of Dispersed Multiphase Flow: Proceedings of an Advanced Seminar, Conducted by the Mathematics Research Center, the University of Wisconsin–Madison, May 26–28, 1982*, 271–289. https://doi.org/10.1016/b978-0-12-493120-6.50017-9.

Barrette, P. D. 2020. "A Tabulated Review of 83 Laboratory Studies on Frazil Ice." In *Proceedings of the 25th International Symposium on Ice. Association of Hydraulic Engineering and Research (IAHR)*, Trondheim, November 23–25. https://www.researchgate.net/publication/346569402_A_tabulated_review_of_83_laboratory_studies_on_frazil_ice.

Beltaos, S., ed. 1995. *River Ice Jams*. Littleton, CO: Water Resources Publications, LLC.

Blackburn, J., and Y. She. 2019. "A Comprehensive Public-Domain River Ice Process Model and Its Application to a Complex Natural River." *Cold Regions Science and Technology* 163:44–58. https://doi.org/10.1016/j.coldregions.2019.04.010.

Boyd, S., T. Ghobrial, M. Loewen, M. Jasek, and J. Evans. 2022. "A Study of Supercooling in Rivers." *Cold Regions Science and Technology* 194:103455. https://www.sciencedirect.com/science/article/pii/S0165232X21002366.

Brunner, G. W. 2016. *HEC-RAS River Analysis System: User's Manual*. CPD-68. Davis, CA: US Army Corps of Engineers, Institute for Water Resources, Hydrologic Engineering Center. https://www.hec.usace.army.mil/confluence/rasdocs/rasum/latest.

Carstens, T. 1970. *Heat Exchanges and Frazil Formation*. In *Proceedings of the Symposium on Ice and its Action on Hydraulic Structures*, Reykjavik, Island, IAHR Paper no. 2.11. https://erdclibrary.on.worldcat.org/oclc/22262488.

Chang, R. 1996. *Essential Chemistry*. New York, NY: McGraw-Hill College.

Daly, S. F. 1984. *Frazil Ice Dynamics*. Monograph 84-1. Hanover, NH: US Army Corps of Engineers, Cold Regions Research and Engineering Laboratory.

Daly, S. F. 1994. *International Association for Hydraulic Research Working Group on Thermal Regimes: Report on Frazil Ice*. Special Report 94–23. Hanover, NH: US Army Corps of Engineers, Cold Regions Research and Engineering Laboratory.

Daly, Steven F., and R. Ettema. 2006. "Frazil Ice Blockage of Water Intakes in the Great Lakes." *Journal of Hydraulic Engineering* 132 (8): 814–824. https://doi.org/10.1061/(asce)0733-9429(2006)132:8(814).

Dean, A. M. 1983. *Lake Water Intakes under Icing Conditions*. Report 83-15. Hanover, NH: US Army Corps of Engineers, Cold Regions Research and Engineering Laboratory.

Ettema, R., M. F. Karim, and J. F. Kennedy. 1984. *Frazil Ice Formation*. Report 84-14. Hanover, NH: US Army Corps of Engineers, Cold Regions Research and Engineering Laboratory.

Ettema, R., G. Kirkil, and S. Daly. 2009. "Frazil Ice Concerns for Channels, Pump-Lines, Penstocks, Siphons, and Tunnels in Mountainous Regions." *Cold Regions Science and Technology* 55 (2): 202–211. https://doi.org/10.1016/j.coldregions.2008.04.008.

FAA (Federal Aviation Administration). 2016. *Aviation Weather Services–Change 2*. Advisory Circular 00-45H. Washington, DC: Federal Aviation Administration, US Department of Transportation.

Gebre, S., K. Alfredsen, L. Lia, M. Stickler, and E. Tesaker. 2013. "Review of Ice Effects on Hydropower Systems." *Journal of Cold Regions Engineering* 27 (4): 196–222. https://ascelibrary.org/doi/10.1061/%28ASCE%29CR.1943-5495.0000059.

Giovando, J., C. Engel, J. Rocks, S. F. Daly, D. O'Connor, and D. Hamill. 2019. *Ice Management Operations at Albeni Falls Dam*. ERDC/CRREL TR-19-21. Hanover, NH: US Army Engineer Research and Development Center, Cold Regions Research and Engineering Laboratory.

Holmgren, William F., Clifford W. Hansen, and Mark A. Mikofski. 2018. "pvlib python: A Python Package for Modeling Solar Energy Systems." *Journal of Open Source Software* 3 (29): 884. https://doi.org/10.21105/joss.00884.

ISU (Iowa State University). 2022. "Iowa Environmental Mesonet." Accessed 08 March 2023. https://mesonet.agron.iastate.edu/.

Lindenschmidt, K. E. 2017. RIVICE–A Non-Proprietary, Open-Source, One-Dimensional River-Ice Model. *Water* 9 (5): 314. https://doi.org/10.3390/w9050314.

Maidment, D. 1993. *Handbook of Hydrology*. New York, NY: McGraw-Hill.

Morales-Marín, L. A., P. R. Sanyal, H. Kadowaki, Z. Li, P. Rokaya, and K. E. Lindenschmidt. 2019. A Hydrological and Water Temperature Modelling Framework to Simulate the Timing of River Freeze-Up and Ice-Cover Breakup in Large-Scale Catchments." *Environmental Modelling and Software* 114 (September 2018) : 49–63. https://doi.org/10.1016/j.envsoft.2019.01.009.

NWS (National Weather Service). n.d. "Automated Surface Observing Systems (ASOS)." Accessed 08 March 2023. https://www.weather.gov/asos/asostech.

NWS. n.d. *National Weather Service*. Accessed 08 March 23. https://www.weather.gov/.

Planet Developers. 2023. "PlanetScope." https://developers.planet.com/docs/data/planetscope/.

Richard, M., B. Morse, and S. F. Daly. 2015. "Modeling Frazil Ice Growth in the St. Lawrence River." *Canadian Journal of Civil Engineering* 42 (9): 592–608. https://doi.org/10.1139/cjce-2014-0082.

USACE (US Army Corps of Engineers). 2002. *Ice Engineering*. EM 1110-2-1612. Washington, DC: Department of the Army.

USACE HEC (US Army Corps of Engineers, Hydrologic Engineering Center). n.d. "HEC-DSS." Accessed 08 March 2023. https://www.hec.usace.army.mil/software/hec-dss/.

USGS (US Geological Survey). 2017. "1/3rd Arc-Second Digital Elevation Models (DEMs)– USGS National Map 3DEP Downloadable Data Collection." Reston, VA: US Geological Survey.

Ye, S. Q., J. Doering, and H. T. Shen. 2004. "A Laboratory Study of Frazil Evolution in a Counter-Rotating Flume." *Canadian Journal of Civil Engineering* 31 (6): 899–914. https://doi.org/10.1139/L04-056.

Zhang, Z., and B. E. Johnson. 2016. *Aquatic Nutrient Simulation Modules (NSMs) Developed for Hydrologic and Hydraulic Models*. ERDC/EL TR-16-1. Vicksburg, MS: US Army Engineer Research and Development Center, Environmental Laboratory.

Appendix A: Temperature Model Results

Figure A-1. Modeled and observed temperatures (in degrees Celsius) for WY 2013, 2015, 2016, 2019, and 2020.

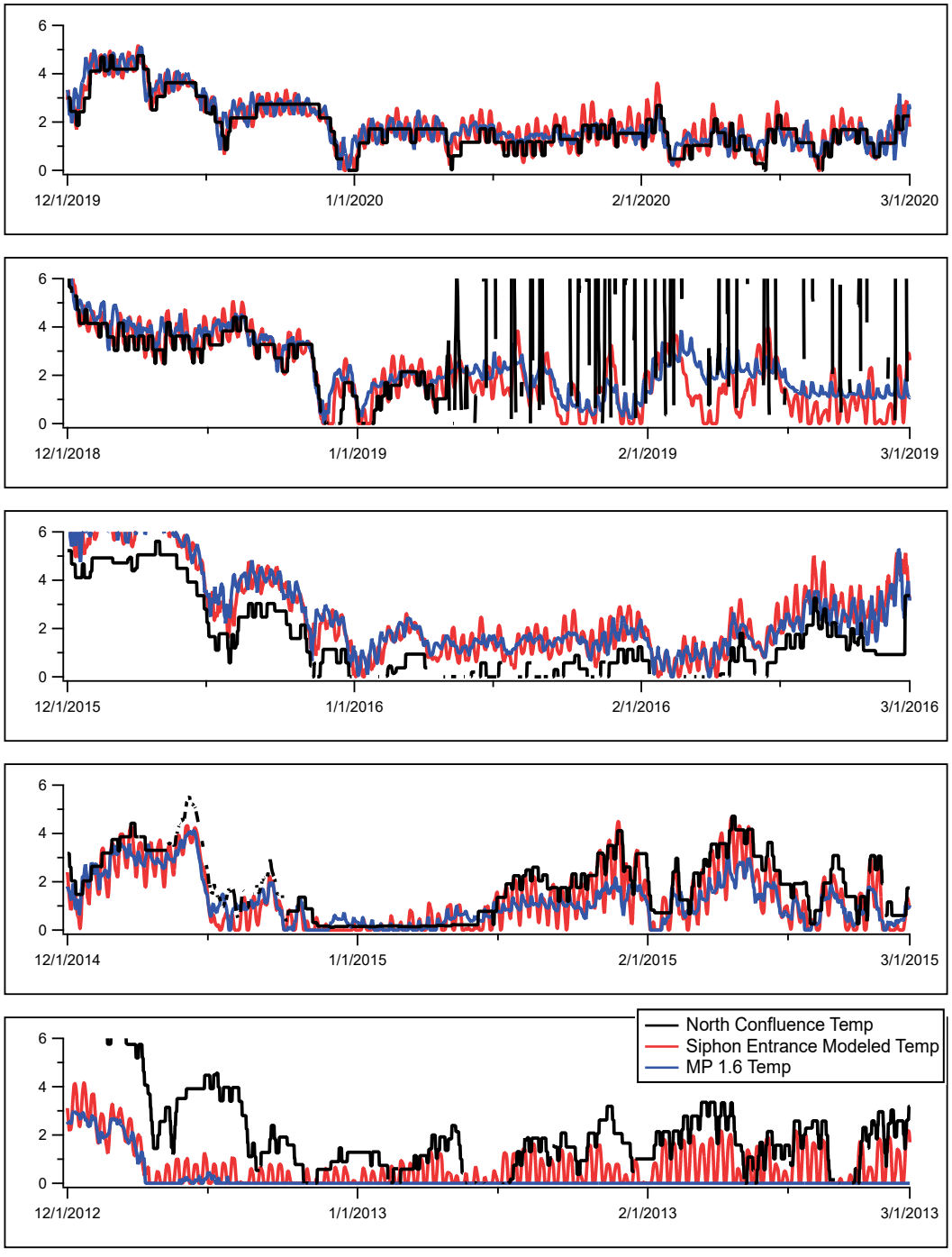

Appendix B: Additional Historical Ice Events

Figure B-1. Net heat flux, canal stage, discharge, and temperature of water in the Sutherland Canal for January and February 2011.

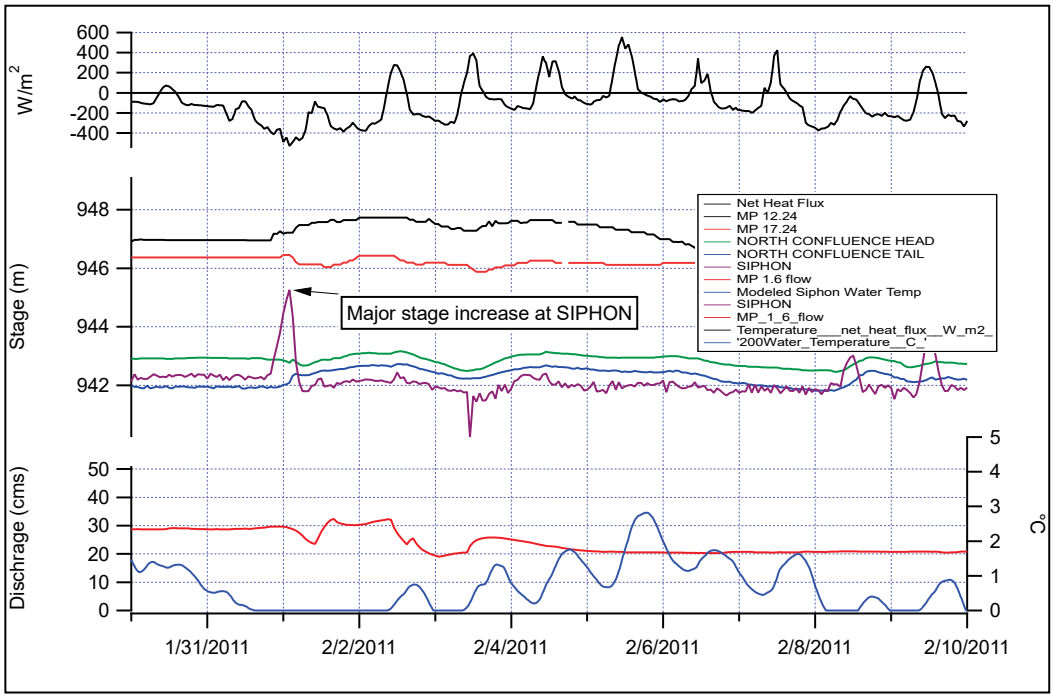

Figure B-2. Net heat flux, canal stage, discharge, and temperature of water in the Sutherland Canal for January 2012.

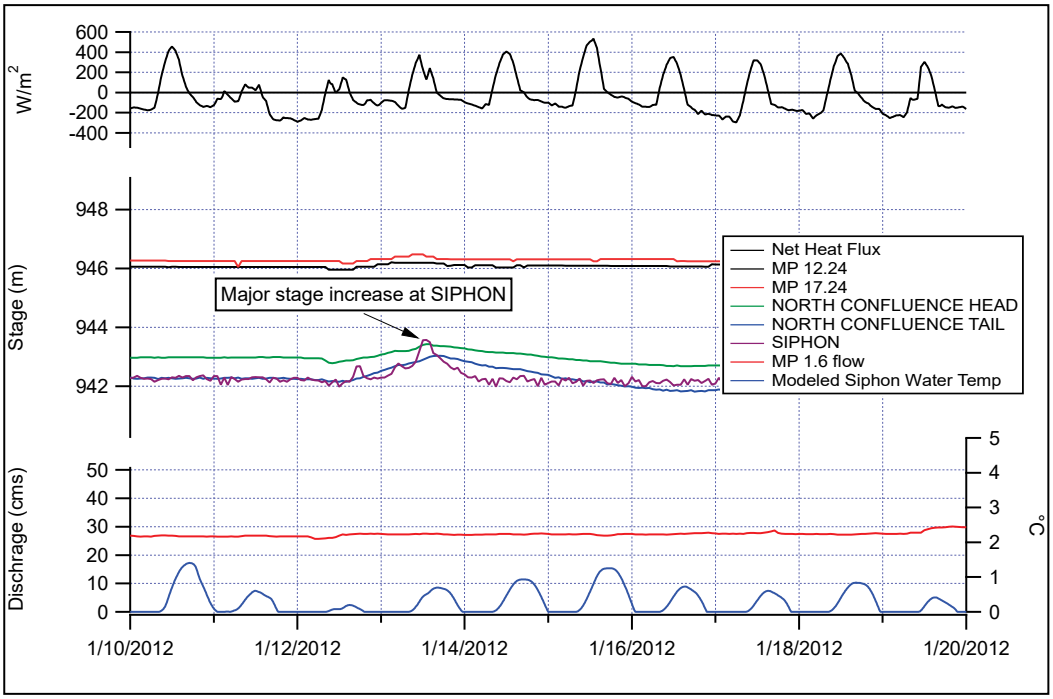

Figure B-3. Net heat flux, canal stage, discharge, and temperature of water in the Sutherland Canal for January 2015.

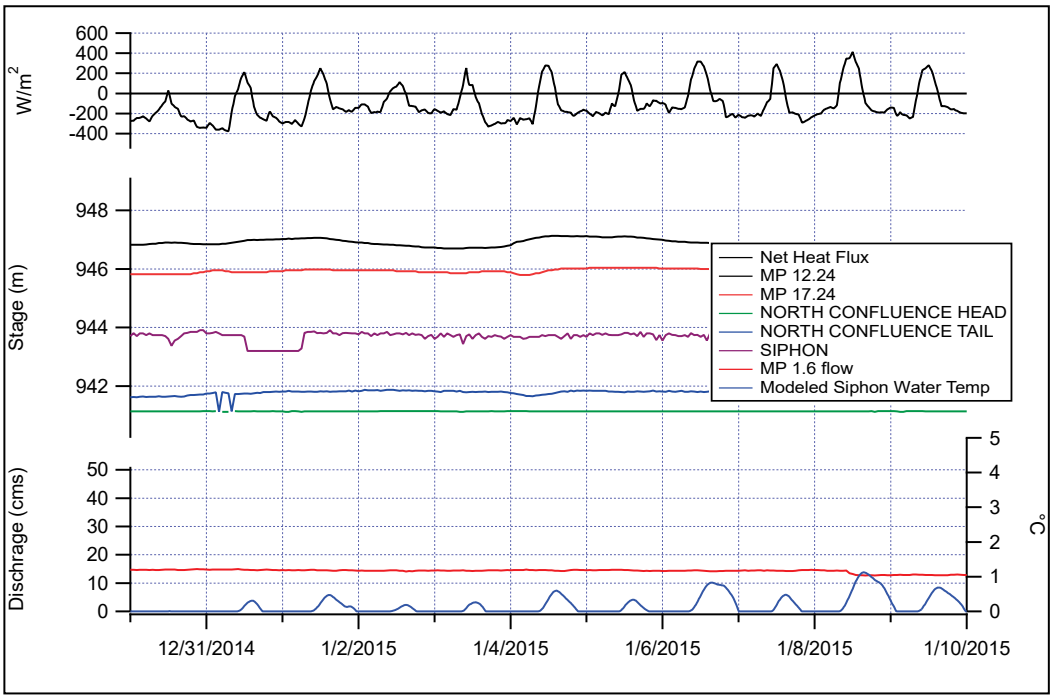

Figure B-4. Net heat flux, canal stage, discharge, and temperature of water in the Sutherland Canal for December 2015.

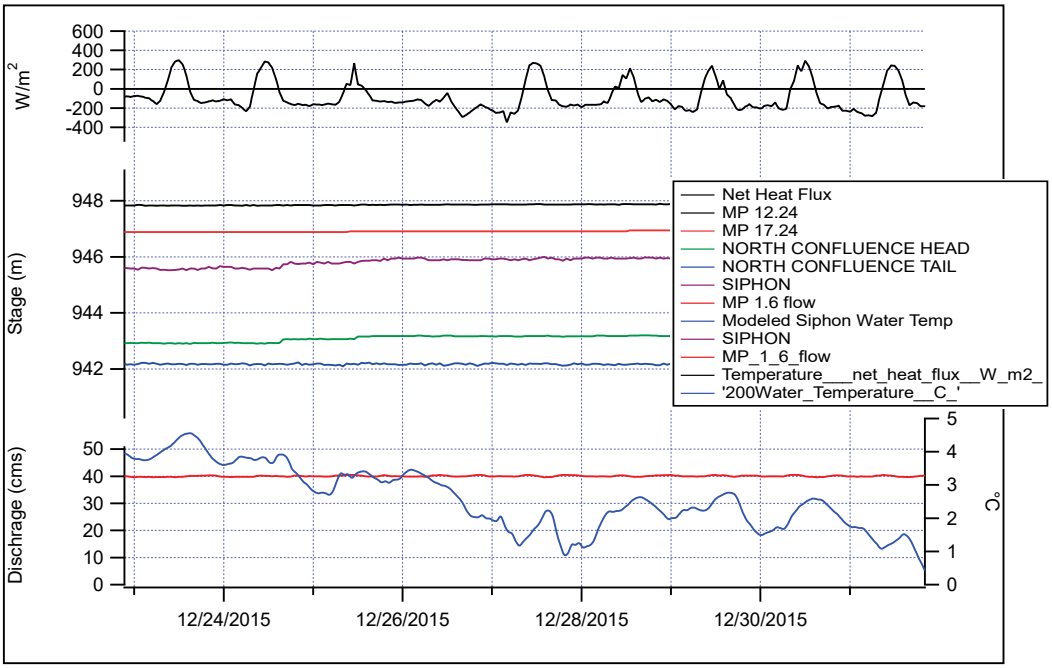

Figure B-5. Net heat flux, canal stage, discharge, and temperature of water in the Sutherland Canal for January 2017.

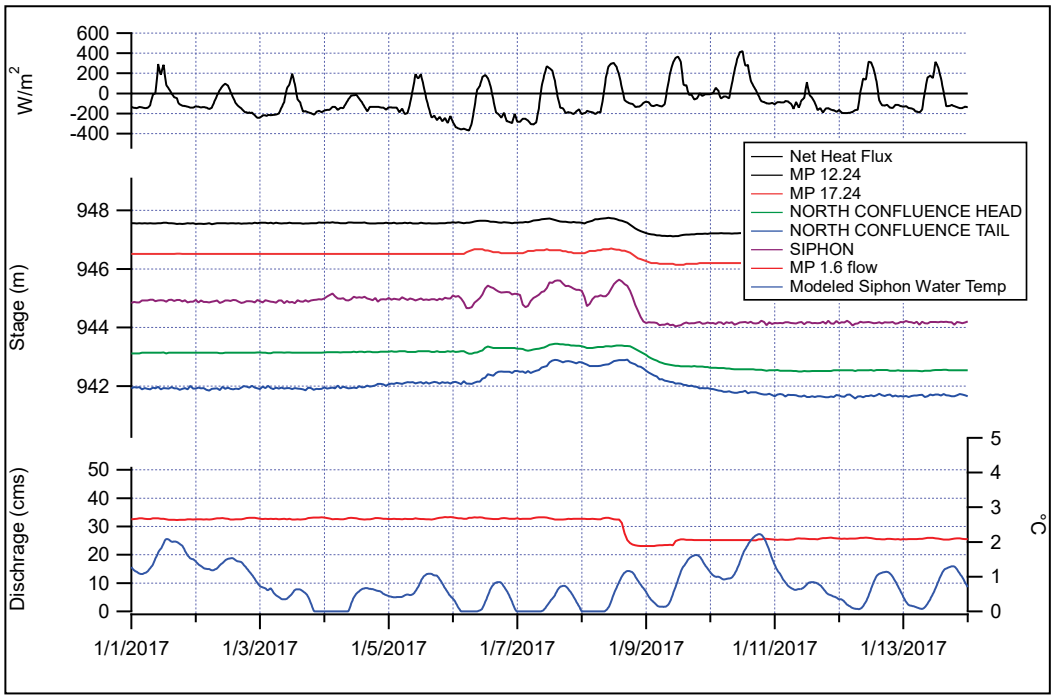

Figure B-6. Net heat flux, canal stage, discharge, and temperature of water in the Sutherland Canal for January 2018.

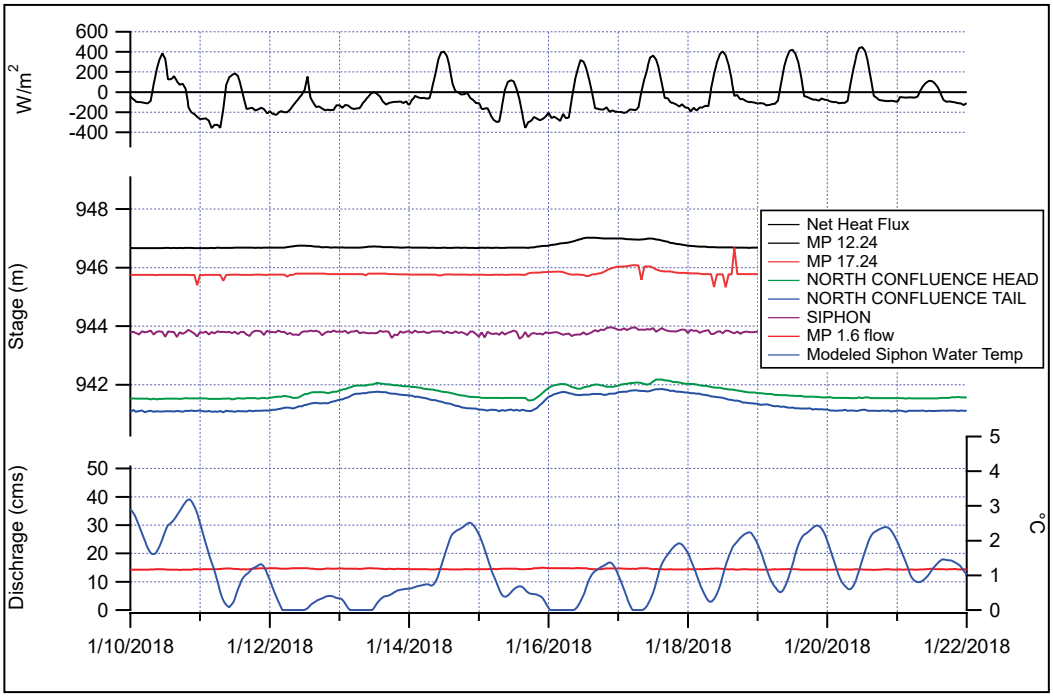

Figure B-7. Net heat flux, canal stage, discharge, and temperature of water in the Sutherland Canal for February 2019.

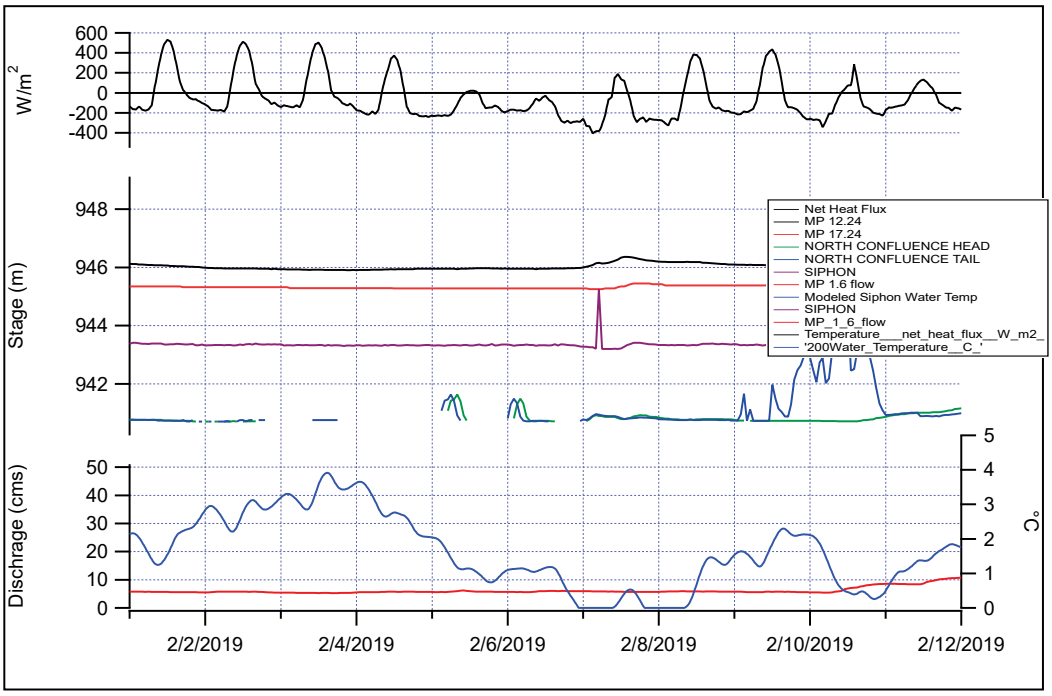

Figure B-8. Net heat flux, canal stage, discharge, and temperature of water in the Sutherland Canal for December 2019.

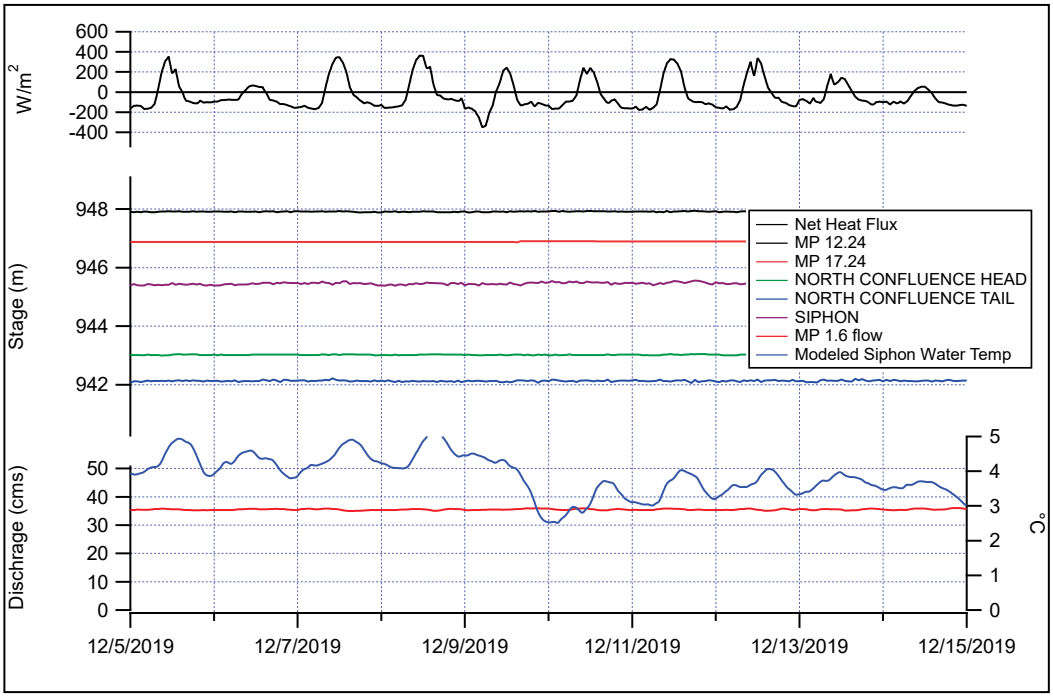

Abbreviations

API	Application programming interface
ASOS	Automated surface observation system
CRREL	Cold Regions Research and Engineering Laboratory
DSS	Data storage system
FAA	Federal Aviation Administration
FERC	Federal Energy Regulatory Commission
GUI	Graphical user interface
HEC	Hydrologic Engineering Center
HEC-RAS	Hydrologic Engineering Center–River Analysis System
HW	Headwater
MAE	Mean absolute error
METAR	Meteorological Aerodrome Reports
MP	Mile post
NPPD	Nebraska Public Power District
NWS	National Weather Service
OGA	Ogallala Municipal Airport
1D	1-dimensional
RAS	River Analysis System
RH	Relative humidity
RMSE	Root mean square error
TW	Tailwater
WY	Water Year

REPORT DOCUMENTATION PAGE

1. REPORT DATE	2. REPORT TYPE	3. DATES COVERED	
		START DATE	END DATE
May 2023	Final report	FY22	FY23

4. TITLE AND SUBTITLE

Analysis of Paxton Siphon Frazil Ice Blockage Event during January 2022

5a. CONTRACT NUMBER	5b. GRANT NUMBER	5c. PROGRAM ELEMENT
5d. PROJECT NUMBER	**5e. TASK NUMBER**	**5f. WORK UNIT NUMBER**

6. AUTHOR(S)
Chandler Engel, Jeremy Giovando, and Grant Halvorson

7. PERFORMING ORGANIZATION NAME(S) AND ADDRESS(ES)	8. PERFORMING ORGANIZATION REPORT NUMBER
See reverse.	ERDC/CRREL TR-23-4

9. SPONSORING/MONITORING AGENCY NAME(S) AND ADDRESS(ES)	10. SPONSOR/MONITOR'S ACRONYM(S)	11. SPONSOR/MONITOR'S REPORT NUMBER(S)
Nebraska Public Power District 1414 15th St Columbus, NE 68602	NPPD	

12. DISTRIBUTION/AVAILABILITY STATEMENT
DISTRIBUTION STATEMENT A. Approved for public release; distribution is unlimited.

13. SUPPLEMENTARY NOTES
MIPR 5J238-19L5JL

14. ABSTRACT
In early January 2022, the Paxton Siphon, owned and operated by the Nebraska Public Power District, filled with frazil ice creating a blockage that resulted in a rapid upstream stage rise for the Sutherland Canal. An event of this type has never happened in the over 80 years of operating the Paxton Siphon. An analysis of the available weather and canal data suggests a rapid air temperature change resulted in the water becoming supercooled, which combined with the moderately low flows in the canal resulted in an anomalous frazil ice formation event. To address this issue for future cold weather events, a water temperature model was developed using the Hydrologic Engineering Center's River Analysis System and can be used to determine the spatial extents of the supercooling event using forecasted weather information. In addition, we developed a heat-exchange forecast tool that can be used operationally to screen for potential frazil ice formation periods with a 1-week outlook period.

15. SUBJECT TERMS
Flood control; Frazil ice; Ice on rivers, lakes, etc.; Lake McConaughy (Neb.); Lake Ogallala (Neb.)

16. SECURITY CLASSIFICATION OF:			17. LIMITATION OF ABSTRACT	18. NUMBER OF PAGES
a. REPORT	b. ABSTRACT	C. THIS PAGE		
Unclassified	Unclassified	Unclassified	SAR	72

19a. NAME OF RESPONSIBLE PERSON	19b. TELEPHONE NUMBER (include area code)
Chandler Engel	601-646-4294

7. PERFORMING ORGANIZATION NAME(S) AND ADDRESS(ES)

US Army Engineer Research and Development Center
Cold Regions Research and Engineering Laboratory
72 Lyme Road
Hanover, NH 03755

US Army Corps of Engineers
St. Paul District
332 Minnesota St, Suite E1500
St. Paul, MN 55101